General Disclaimer

One or more of the Following Statements may affect this Document

- This document has been reproduced from the best copy furnished by the organizational source. It is being released in the interest of making available as much information as possible.

- This document may contain data, which exceeds the sheet parameters. It was furnished in this condition by the organizational source and is the best copy available.

- This document may contain tone-on-tone or color graphs, charts and/or pictures, which have been reproduced in black and white.

- This document is paginated as submitted by the original source.

- Portions of this document are not fully legible due to the historical nature of some of the material. However, it is the best reproduction available from the original submission.

Produced by the NASA Center for Aerospace Information (CASI)

On the Causes of Geomagnetic Activity

by

Leif Svalgaard

December 1975

Reproduction in whole or in part is permitted for any purpose of the United States Government.

MAR 1976
RECEIVED
NASA STI FACILITY
INPUT BRANCH

SUIPR Report No. 646

Office of Naval Research
Contract N00014-76-C-0207

National Aeronautics and Space Administration
Grant NGR 05-020-559

and

National Science Foundation
Grant ATM74-19007

INSTITUTE FOR PLASMA RESEARCH
STANFORD UNIVERSITY, STANFORD, CALIFORNIA

(NASA-CR-146295) THE CAUSES OF GOEMAGNETIC ACTIVITY (Stanford Univ.) 49 p HC $4.00 CSCL 08N
N76-18720
Unclas
G3/46 18261

ON THE CAUSES OF GEOMAGNETIC ACTIVITY

Leif Svalgaard
Institute for Plasma Research
Stanford University
Stanford, California
94305

Abstract

The causes of geomagnetic activity are studied both theoretically in terms of the reconnection model and empirically using the am-index and interplanetary solar wind parameters. It is found that two separate mechanisms supply energy to the magnetosphere. One mechanism depends critically on the magnitude and direction of the interplanetary magnetic field. Both depend strongly on solar wind speed. The energy input is modulated by the tilt of the dipole axis being maximum for 90^{o} tilt against the solar wind flow direction. The energy input due to reconnection has no significant seasonal or UT variations for equal amount of both sector polarities.

ON THE CAUSES OF GEOMAGNETIC ACTIVITY

Leif Svalgaard
Institute for Plasma Research
Stanford University
Stanford, California
94305

Introduction

Geomagnetic activity could - following J. Bartels - be defined as the short-term effects on the geomagnetic field of the variable solar wind. Despite the difference between our present understanding and Bartels' original ideas when the K-index was introduced (Bartels et al., 1939) the K-index and derived indices are generally appreciated and widely used by researchers in a variety of fields. By combining local K-indices from a network of stations into the planetary index Kp, Bartels strived at devising a quantitative measure for the intensity of the "Partikelstrahlung" from the sun. We now know that the interplanetary magnetic field is an important property of the solar wind in generating geomagnetic activity (Schatten and Wilcox, 1967). This means that the geomagnetic indices also reflect properties of the interplanetary magnetic field and of the solar magnetic field.

The imbedded magnetic field gives the solar wind plasma fluid properties so that frictional or viscous-like interactions can take place between the streaming solar wind and the magnetosphere. Furthermore, the amount of magnetic flux in the magnetotail has been found to depend on the direction of the interplanetary magnetic field (see review by Burch, 1974). If the interplanetary magnetic field has a component that is antiparallel to the geomagnetic field lines on the sunward side of the magnetosphere, it can readily connect with the terrestrial field and is then swept back into the tail by the streaming of the solar wind. The magnetic energy in the stretched-out field lines is then stored in the magnetotail for later release as geomagnetic activity. The energy release - often manifested as substorms - may be triggered by instabil-

ities of the tail configuration. Such instab lities may have causes internal to the tail as well as being excited by external events in the ever changing solar wind. The Kelvin-Helmholtz instability of the boundary between two magnetodynamic fluids has often been proposed (e.g. Boller and Stolov (1970)) to be responsible for at least some geomagnetic disturbances. Compression of the magnetosphere by increased solar wind pressure may also play a role in triggering the energy releases.

Because the rotation axis of the Earth is inclined by $23^{\circ}.5$ to the Ecliptic and the geomagnetic dipole axis in turn is inclined $11^{\circ}.4$ to the rotation axis, the angles between the average interplanetary magnetic field and between the solar wind direction and the geomagnetic field both vary seasonally and daily. These variations should give rise to both seasonal and diurnal variations of the geomagnetic activity. Such variations exist, of course, and have been extensively discussed in the literature.
The semiannual variation was discovered by Broun (1874) from observations of the Declination at Trivandrum. Recent discussions include Mayaud (1970), Wilcox (1968), Boller and Stolov (1970), Siebert (1971), Saito (1972), Russell and McPherron (1973), and Meyer (1974).
The importance of these regular variations lies in the possibility to discriminate between several theories or models of the modes of interaction between the solar wind and the magnetosphere. Furthermore, if the correct model (or models) can be singled out, the more than century-long monitoring of the geomagnetic field could provide insight into the long-term features of the source of geomagnetic activity: the magnetic field of the sun.

In spite of the rich literature on the subject there appears to be some confusion in regard to the precise nature of the seasonal and diurnal variations of geomagnetic activity (Russell and McPherron, 1974). Part of this confusion arises from the fact that the variations predicted by specific models do not agree with observations thus making interpretation of the data difficult. It is the purpose of the present study to clarify the situation and to show that the observed variations may be interpreted in a way that is consistent with our present understanding of magnetospheric processes.

Data Description

As a measure of geomagnetic activity we shall use the am index introduced by Mayaud (1967). This index is a three-hour index character-

izing the world wide level of activity on a linear scale, giving essentially the amplitude in nanoTesla (1nT=1 gamma) of the irregular deviations during that three-hour interval of the horizontal component from the regular daily variation. Several geomagnetic observatories are grouped into groups that have uniform distribution in longitude. There are five groups in the northern hemisphere and three in the southern. By averaging the deviations first for each group separately and then averaging the group means for each hemisphere, indices an and as result. The am index is then defined as am = (an + as)/2. This procedure largely removes local time effects - in particular the uneven illumination of the auroral zones. The resulting index, am, can therefore be considered to be a close approximation to a true planetary index. In the present analysis we utilize the am indices derived for the interval 1962-70.

The interplanetary magnetic field has been monitored extensively since the Mariner-2 flight in 1962. The magnetic field is carried out from the sun by the radially expanding solar wind and is curved by solar rotation into a spiral on a conic surface with the focal line along the solar rotation axis. The field is organized into sectors where the field points predominantly either toward the sun or away from the sun along the spiral (Wilcox, 1968). During most three-hour intervals it is possible to assign a definite polarity to the field. In addition we compute the average field latitude angle and magnitude for these three-hour intervals. By using three-hour averages we get quantities that may be compared directly with the am index. A disadvantage of the averaging is that the variability of the field is somewhat suppressed. The interplanetary data was obtained from compilations by Wilcox and Colburn (1972) and from the National Space Science Data Center.

The use of planetary indices for studying the Universal Time variation of geomagnetic activity has been questioned by Russell and McPherron (1974) on the basis that these diurnal variations are sensitive to the definition of the index and that different indices show different diurnal variations. Such differences arise from uneven station distributions and imperfect weighting factors when many stations are combined into a planetary index. Such complications are largely avoided in the construction of the am-index, which Mayaud claims to be a fair approxi-

mation to a true planetary index. It is possible to verify this claim by comparing the UT variations on days with opposite polarity of the interplanetary magnetic field. As we shall discuss at length in later sections of the paper, we would expect UT variations that are roughly sinusoidal but in antiphase for the two opposite polarities, away from or towards the sun. Such UT variations are indeed exhibited by the am-index as shown in Figure 1.

Even the an- and as-indices separately show the same UT variation as the am-index. A minor distortion of the curves for the two separate hemispheres results from the antipodal character of the polar caps, but may be removed by computing the differences between the variation during away polarity and the variation during toward polarity. These difference curves are virtually identical for all three indices as shown in the right-hand panel of Figure 1. In this connection it should be pointed out that the an- and the as-indices are completely independent. They are derived from different sets of stations with different longitudinal distributions. Yet the difference curves have the same phase and amplitude for each index. This result leaves no doubt that real UT variations exist and that the am-index does indeed exhibit these variations. These UT variations have - as we shall show - the correct phase and amplitude to be explained by diurnal changes in the amount of interplanetary magnetic flux reconnecting to the magnetosphere but are distinctly different from the UT variations described by Mayaud (1970) obtained by not separating the data according to sector polarity. Both systems of variations exist, however, and a similar co-existence of two separate systems of semiannual variations will also be demonstrated. In fact we shall show that there co-exist two different systems of geomagnetic variations. One system depends on the direction of the interplanetary magnetic field whereas the other system depends on the angle between the solar wind direction and the earth's dipole axis. The first system has no significant semiannual or diurnal variations when about the same number of days with each polarity are averaged together. The second system, that is independent of the direction of the interplanetary magnetic field, shows the well known classical semiannual variation and the diurnal variations so aptly described by McIntosh (1959) and Mayaud (1970).

Analysis of am-variations

A property of the classical UT variation of geomagnetic activity (McIntosh, 1959) is that the phase of the variation changes with season.

At the two solstices the variations are precisely in antiphase, while at the equinoxes the UT variations are very much smaller having two maxima and two minima. Averaged over all seasons the resulting UT variations are very small and hardly detectable. These are all well known results and make the division of the data into two groups with opposite sector polarity meaningful in the sense that any differences between the geomagnetic response to different polarity will hardly be distorted if averages are taken over all seasons. Any such distortion may also be eliminated if the difference between the UT variations on days with opposite polarities is computed. We saw a nice example of this in the right-hand panel of Figure 1. Because the UT variations have opposite phase for opposite polarity, these variations will cancel out when all days are averaged without regard of the sector polarity. Proper selection of averaging parameters may thus isolate different components of geomagnetic activity that may be excited by or modulated by different processes.

Thus, if the difference between the variations of activity for the two opposite sector polarities is computed, we isolate variations depending critically on just the sector polarity, and if the average variation for all days (strictly: the same number of days of each polarity) is computed we isolate variations essentially independent of the polarity. Figure 2 shows this program carried out for different seasons. We note that the polarity dependent UT variation is essentially independent of seasons, while the polarity independent variations display the well known McIntosh-effect with a reversal of the phase between the two solstices. The amplitudes of the two variations are comparable; the polarity dependent variation being about 70% of the polarity independent variation averaged over the four months intervals of Figure 2.

Figure 3 demonstrates that the classical semiannual variation is independent of polarity but that the differences between activity on away days and on toward days has an annual variation. Again we are finding that geomagnetic activity responds to the sector polarity with two variations that are in antiphase for the two polarities. Such variations have already been noticed by Burch (1973) and by Siscoe and Otaela, and have been used by Russell and McPherron (1973) as support for their notion

that the semiannual variation arises from the superposition of two annual activity waves: one for toward polarity with maximum in April and one for away polarity with maximum in October. At first sight such superposition of two variationsin antiphase should lead to a cancellation of the variations resulting in no semiannual variation at all. Russell and McPherron (1973) avoid this by assuming that there is no interaction between the interplanetary magnetic field and the geomagnetic field when the interplanetary field has a northward component as seen by the magnetosphere. This assumption leads to a model that predicts that activity is confined to only one polarity at each equinox, namely toward polarity in March-April and away polarity in September-October, thus assuring a semiannual variation. However, Figure 4 shows that such behavior is not observed for the UT variations where the variations are always present with almost constant amplitude and phase throughout the year. In Figure 4 we compare the UT variations for the two polarities at times of the year where they should both be large (left-hand panel) and at times where, according to Russell and McPherron (1973), the variations should both be absent or at least very weak (right-hand panel). In fact, the UT variations are equally well present in both panels with no significant difference between them. Thus we find that the variations of geomagnetic activity that depend solely on sector polarity are almost equal in amplitude but opposite in phase for the two polarities. In the following section we show theoretically that such behavior is just what might be predicted from a simple treatment of the geometry of the reconnection process at the dayside of the magnetosphere.

At this point it is worth mentioning that the finding of opposite UT variation for different sector polarity can be used as a sensitive vehicle for testing the accuracy of polarities inferred from polar geomagnetic records (e.g. Svalgaard, 1972; Wilcox, 1972). The amplitude of the UT variation for a given inferred polarity is presumably less than - say a fraction f of - the amplitude of the variation we would find had the polarities been measured by spacecraft. This is due to the fact that only a fraction p of the days are inferred correctly, where

$$p = (1+f)/2 \qquad (1)$$

Actually p would be a lower limit for the success rate depending on the time resolution of the inferred polarities because of short-period fluctuations of the sector polarity.

Dayside reconnection model

The discussion will be focused on the process of magnetic merging or field line reconnection. It is now widely accepted that this process plays a crucial role in determining the topology of magnetic fields and plasmas and provides the most plausible way of releasing energy stored in a magnetic field in order to produce large dissipative events. A critical review of the fundamental physics of magnetic field line merging has recently been given by Vasyliunas (1975).

For the magnetic field configuration in and around the earth's magnetosphere we distinguish three classes of field lines: (1) closed field lines that connect to the earth in both directions, (2) open field lines that connect to the earth at one end and to interplanetary space at the other end, and (3) interplanetary field lines that do not connect to the earth at all. The regions of space traversed by the different classes of field lines are bounded by a surface called the separatrix. The intersection of the separatrix with the noon-midnight meridian plane is shown in Figure 5 as a heavy line. The separatrix could be visualized, topologically, as a doughnut touching the inside of a cylinder. Thus, the separatrix has two branches (the doughnut and the cylinder) intersecting along a line commonly called the X line. In general there is a magnetic field component along the X line.

Any change of the amount of magnetic flux connecting the earth with interplanetary space (i.e. the sun!) will require magnetic flux transport across the separatrix which in turn also implies a plasma flow across the separatrix. This plasma flow is the essential element in the definition of the merging concept as applied to large-scale plasma systems: "Magnetic field line merging, or reconnection, is the process whereby plasma flows across a surface that separates regions containing topologically different magnetic field lines" (Vasyliunas, 1975).

The coupling between the plasma flow and the transport of magnetic flux is provided by an electric field $\underset{\sim}{E}$ given by

$$\underset{\sim}{E} + \underset{\sim}{V} \times \underset{\sim}{B} \simeq 0 \qquad (2)$$

where $\underset{\sim}{B}$ is the magnetic induction field and $\underset{\sim}{V}$ is the bulk flow velocity of the plasma. Equation (1) states that there be no electric field in the frame moving with the plasma ($\underset{\sim}{V} = 0$), and also implies that any plasma flow across magnetic field lines (such as the ones making up the separatrix surface) is associated with an electric field lying in the separatrix surface at right angles to $\underset{\sim}{B}$. The existence of such an electric field is thus an alternative way of stating that magnetic merging is occurring.

The geomagnetic field presents an obstacle to the solar wind flow and introduces field lines with different topologies in the region surrounding the earth. Magnetic merging at the magnetopause is one process by which the solar wind can pass through the magnetosphere obstacle. Merging is associated with an electric field across the magnetosphere along the X-line, perpendicular to the geomagnetic field earthward of the X-line and hence pointing from the dawn side to the dusk side of the magnetosphere. The field lines that reconnect on the dayside magnetosphere are stretched back by the solar wind into the magnetotail of Length T until the two branches of tail field lines (one from each hemisphere) meet and connect again. In this way the interplanetary magnetic field lines pass through the magnetosphere and the geomagnetic field lines gain tensional energy. The total amount of tensional energy gained by these field lines represents an effective energy transfer to the magnetosphere owing to merging at the magnetopause.

The power transferred to the magnetosphere is the integral of the Poynting vector $\underset{\sim}{E} \times \underset{\sim}{H}$ over the doughnut-part of the separatrix surface S:

$$P = \int d\underset{\sim}{S} \cdot (\underset{\sim}{E} \times \underset{\sim}{H}) \tag{3}$$

or approximately (ignoring the dayside part):

$$P = \frac{2k}{\mu_o} \int dX dY E_Y B_X \tag{4}$$

where k is of the order of unity. We consider the tail to be a cylinder with its axis in the X-direction and having a width 2R in the Y-direction in the ecliptic. E_Y is the cross-tail electric field due to reconnection and $B_X = \mu_o H_X$ is the magnetic induction field in the tail. The potential difference between the dusk side and the dawn side of the magnetosphere is $\Phi = \int dY E_Y$, and we may write:

$$\int dX B_X = B_T T \tag{5}$$

where B_T is an appropriate average field strength in the tail. Observationally B_T is of the order of 10 nT and is found to be very nearly parallel to the tail axis. We can therefor express the power supplied to the magnetosphere by the solar wind as

$$P = \frac{2k}{\mu_o} \Phi B_T T \qquad (6)$$

A similar result can be obtained by treating each tail lobe as a solenoid. A surface current must flow around each lobe to maintain the magnetic configuration, especially to keep the two lobes apart. The solenoidal currect density required is $j = B_T/\mu o$ per lobe, or $2j \cdot T$ for the total current across the tail. The amount of energy drawn from the solar wind by this current over a potential difference Φ is

$$P = (2j \cdot T)\Phi = \frac{2}{\mu o} \Phi B_T T$$

Again a geometrical factor like k may be applied to account for the details of the circuit geometry.

If magnetic merging takes place predominantly in a region of width D around the nose of the magnetosphere where the solar wind flow is nearly normal to the magnetopause, the electric field associated with the merging is then of the order $E = VB$ and the potential drop across the reconnection region is $\Phi = E \cdot D = VBD$. This potential difference can be thought of as the number of field lines approaching the merging region per unit time. We assume that there is no restriction on the merging rate, i.e. that all field lines frozen into plasma flowing through the separatrix do indeed reconnect. Otherwise we would encounter a topologically unpleasing field configuration. We can therefore state that the potential drop across the merging region is equal to the number of interplanetary field lines reconnecting per unit time on the dayside.

It takes the solar wind the time T/V to pass the magnetosphere (because $T \gg$ dayside stand-off distance). The total number of field lines reconnected during that time is then $\Phi T/V$. In a steady state this will be the amount of open magnetic flux in each tail lobe. The field strength in the tail lobe is then $\Phi T/V$ divided by the cross-sectional area of the high latitude region of the lobe taken to be $\frac{1}{2}\pi R^2$ giving

$$P_T = \frac{2\Phi T}{\pi R^2 V} \tag{7}$$

Combining (3) and (4) we get an expression for the power input

$$P = \frac{2k}{\pi \mu_o} \cdot \frac{T^2}{R^2 V} \Phi^2 \tag{8}$$

So far in our discussion we have assumed that the interplanetary magnetic field B_I was antiparallel with the geomagnetic field B_G near the dayside X-line. If the two fields make an arbitrary angle α with each other, the antiparallel components of the two fields (if they exist) now determine how many field lines can reconnect. From the geometry of Figure 6 it follows that the antiparallel component of B_I is given by

$$B = B_I \sin u$$

$$= B_I \frac{B_I - B_G \cos \alpha}{(B_G^2 + B_I^2 - 2B_I B_G \cos \alpha)^{\frac{1}{2}}}$$

$$= B_I \frac{s - \cos \alpha}{(1 + s^2 - 2s\cos \alpha)^{\frac{1}{2}}} \tag{9}$$

where $s = B_I/B_G$, provided that $\cos \alpha < s$. If $\cos \alpha \geq s$, no antiparallel components exist and merging becomes geometrically impossible. Similar ideas have been developed previously by Gonzalez and Mozer (1974) and by Sonnerup (1974). Using (9) we get:

$$\Phi = DVB_I \frac{s - \cos\alpha}{(1 + s^2 - 2s\cos\alpha)^{\frac{1}{2}}} \quad , s > \cos\alpha \tag{10}$$

By using the concept of a plane merging region of width D instead of the (unknown) real three-dimensional configuration, we are hiding our ignorance about the actual magnetosheath flow pattern behind a geometrical factor f, such that $D = fR$. The main reason that we expect f to be rather small is that the magnetosheath plasma flow rapidly becomes tangential to the magnetopause when we move away from the solar wind stagnation point at the nose of the magnetosphere. When this happens, the solar wind has in a sense already passed the geomagnetic obstacle.

Up to now, we have ignored the presence of the bow shock upstream of the magnetosphere. The solar wind is slowed down at the shock front to magnetosheath values V_M and the field strength is increased to B_M. The magnetic flux transport is largely unaltered so that $VB_I \simeq V_M B_M$, and we will continue to use VB_I in lieu of $V_M B_M$. But in defining s as the ratio between

the magnetic field strengths just outside and just inside of the magnetopause we should use B_M rather than B_I, i.e.

$$s = B_M/B_G$$

Observationally s is found to be near $\frac{1}{2}$ rather independent of B_M. The explanation may be that increased B_M leads to "erosion" of the dayside magnetosphere due to enhanced reconnection. The magnetopause thus moves closer to the earth so that B_G also increases, keeping s nearly constant.

An estimate of the geometrical factor f determining the size of the merging region may be obtained by equating Φ determined from (7) to Φ as given by (10). Assuming $\alpha = 90^o$, the result becomes

$$f = \frac{B_T}{B_I} \frac{R}{T} \frac{\pi(1+s^2)^{\frac{1}{2}}}{s^2} \simeq 0.17 \qquad (11)$$

We have used B_T=11nT, B_I=5nT, R=25R_E, T=1000R_E and s=0.6.
With the definition

$$q(\alpha,s) = \begin{cases} 0 & , \quad s \leq \cos\alpha \\ \dfrac{(s-\cos\alpha)^2}{1 + s^2 - 2s\cos\alpha} & , \quad s > \cos\alpha \end{cases} \qquad (12)$$

and using (8) and (10) we obtain the following expression for the energy transferred to the magnetosphere per unit time:

$$P = \frac{kf^2}{\pi\mu_o} (T^2 V) B_I^2 q(\alpha,s) \qquad (13)$$

With k ≃1, f ≃0.17 and V = 400 km/s we obtain the following numerical estimate

$$P = 1.2 \times 10^{11} B_I^2 q(\alpha,s) \text{ watts} \qquad (14)$$

Where B_I is expressed in nanoTesla. For average values of B_I, α and s we find $\bar{P} \simeq 0.8 \times 10^{12}$ watts = 0.8 TW. Thus in a quiet steady state reconnection constitutes a power transfer from the solar wind to the magnetosphere of the order of 1 terawatt.

We shall now consider consequences of the tendency of the interplanetary field to be organized in large-scale sectors of alternating polarity - toward the sun or away from the sun along the basic field line spiral. Walters (1964) first suggested that the interplanetary magnetic field would be "draped" (Fig. 7) around the sunward part of the magnetosphere. Fairfield (1967) presented observations of the magnetosheath magnetic field, confirming the draping concept. It was further found that the latitude angle of the field is not changed significantly by the draping. The result is then that the magnetic field just outside the magnetopause is tangential to the magnetopause - directed from dawn to dusk in case of an ideal away polarity and from dusk to dawn in case of toward polarity. In addition the field may make a non-zero angle, β, with the ecliptic. Figure 8 shows the orientations of a geomagnetic field line and a interplanetary field line for the two sector polarities. The circles delimit the merging region at the nose of the magnetosphere as seen from the sun. A geomagnetic field line is indicated by the arrow SN having a tilt A to the ecliptic EE. The angles α_A and α_T between the field directions are given by

$$\alpha_A = A - \beta \ , \qquad \alpha_T = 180 - (A+\beta) \tag{15}$$

where β is the ecliptic latitude angle of the interplanetary magnetic field.

Using (14) we can express the power input during the times of away polarity as

$$P_A = pB_I^2 q(\alpha_A, s) \tag{16}$$

where

$$p = \frac{4kf^2}{\pi\mu_o}(T^2V) \tag{17}$$

Similarly we get for toward polarity

$$P_T = pB_I^2 \, q(\alpha_T, s) \tag{18}$$

The difference between the power input on away days, (i.e. extended intervals where the earth is immersed in an away sector) and on towards days is then proportional to (assuming pB_I^2 to be independent of polarity)

$$\delta_{AT} = \bar{q}(\alpha_A, s) - \bar{q}(\alpha_T, s) \tag{19}$$

The averages in (19) are to be extended over the duration of the intervals in question. The average value of the latitude angle β is $\approx 0^o$; this means

that

$$\cos \alpha_A = \cos (A-\beta) = \cos A$$
$$\cos \alpha_T = -\cos (A+\beta) = -\cos A$$

so that (using (13), followed by some algebraic manipulation):

$$\delta_{AT} = -4sQ(A,s)\cos A \qquad (20)$$

where the auxilliary function $Q(A,s)$ is defined by

$$Q(A,s) = \frac{1 - \cos^2 A}{(1 + s^2)^2 - 4s^2\cos^2 A}$$

$$= \frac{1}{(1+s^2)^2}\left\{1 - (1-s^2)^2 \sum_{n=1}^{\infty} \frac{(4s^2)^{n-1}}{(1+s^2)^{2n}} \cos^{2n} A\right\} \qquad (21)$$

In deriving (20) we have made use of the identity $(s\pm\cos A)^2 = (1+s^2\pm 2s\cos A) - (1-\cos^2 A)$. If, during an extended period (e.g. weeks), away polarity and toward polarity occur with equal probability we can meaningfully define the average power input which is proportional to

$$\sigma_{AT} = (\bar{q}(\alpha_A,s) + \bar{q}(\alpha_T,s))/2$$
$$= 1 - (1+s^2)\ Q(A,s) \qquad (22)$$

For $s=0.6$ (a value discussed later) the first 4 terms in the expansion for Q are

$$Q(A,s) = 0.541 - 0.120 \cos^2 A - 0.093 \cos^4 A - 0.073 \cos^6 A - \ldots (23)$$

Because $\cos A \leq 0.5$, the series converges rapidly and we can ignore the complications caused by $s \leq \cos\alpha$. Corresponding series for δ_{AT} and for σ_{AT} are

$$\left.\begin{aligned}\delta_{AT} &= -1.298 \cos A + 0.287 \cos^3 A + 0.223 \cos^5 A + 0.174 \cos^7 A + \ldots \\ \sigma_{AT} &= 0.265 + 0.163 \cos^2 A + 0.127 \cos^4 A + 0.099 \cos^6 A + \ldots\end{aligned}\right\} \qquad (24)$$

The first term in each of these expansions always dominates, so that to first order

$$\left.\begin{aligned}\delta_{AT} &= -1.298 \cos A \\ \sigma_{AT} &= 0.265 \qquad (= \text{constant})\end{aligned}\right\} \qquad (25)$$

We are thus led to the interesting conclusion that the average power input σ_{AT} to the magnetosphere is nearly constant and thus does not depend on A. The angle A is the angle between geomagnetic field lines in the merging region and the dusk-dawn direction or what is the same the direction opposite the Earth's orbital motion. This angle varies both daily and seasonally but since σ_{AT} does not depend on it to first order, the theory presented here predicts that there be no significant diurnal or seasonal variation of the average power input to the magnetosphere. On the other hand, δ_{AT} or the difference between the power input during away polarity and the input during towards polarity, does depend considerably on A.

To determine the diurnal and seasonal variation of the angle A, reference is made to the spherical geometry in Figure 9. From the spherical triangle SMT we get

$$\cos A = \cos \chi / \sin \psi \tag{26}$$

where ψ is the tilt of the dipole axis to the solar wind direction (ignoring for the moment the 4° abberation due to the motion of the Earth). The angle λ is the ecliptic longitude of the mean sun given by

$$\lambda(d) = 279^{\circ}.69 + 360^{\circ}(d-0.5)/365.24 \tag{27}$$

where d is the day of the year (Jan. 1 ≡1) and λ refers to 12^{h}UT of the day. The dipole axis MO rotates once around OG in the course of one siderial day so that the angle h becomes

$$h = 360^{\circ}(t-10.65)/24 + \lambda \tag{28}$$

where t is Universal Time in hours (mean solar time). The constant $10^{h}.65$ is determined by the geographical longitude of the magnetic pole.

Using the cosine-relation for the spherical triangle SUM we get

$$\cos \psi = \sin\lambda\cos\zeta + \cos\lambda\sin\zeta\cos u$$

and similarly

$$\cos\chi = \cos\lambda\cos\zeta - \sin\lambda\sin\zeta\cos u$$

The auxillary arc ζ can be determined from ΔMUG:

$$\cos\zeta = \cos i \sin\epsilon - \sin i \cos\epsilon \cos h \tag{29}$$

where $\epsilon = 23^{\circ}.45$ is the obliquity of the ecliptic and $i = 11^{\circ}.44$ is the geographical co-latitude of the magnetic pole. Using the sine-relations for ΔMUG we get

$$\sin\zeta \cos u = \sin i \sin h$$

leading to the final expressions for $\cos\psi$ and $\cos X$:

$$\cos\psi = \sin\lambda\cos i \sin\varepsilon - \sin i (\sin\lambda\cos\varepsilon \cosh - \cos\lambda \sin h) \qquad (30)$$

$$\cos X = \cos\lambda \cos i \sin\varepsilon - \sin i (\cos\lambda\cos\varepsilon \cosh + \sin\lambda \sinh) \qquad (31)$$

The first term in each expression gives the purely seasonal variation of the angles while the second term determines the diurnal modulation.

We note that $\cos\psi$ and $\cos X$ are the components of a unit vector along OM (opposite the dipole axis) on the X- and the Y- directions respectively. The Z- component is easily found to be

$$\cos T = \cos\varepsilon \cos i + \sin\varepsilon \sin i \cosh \qquad (32)$$

Comparing the model with observations

Having derived expressions for the energy transferred to the magnetosphere by the solar wind we now make the assumption that some of the energy transferred to the magnetosphere is dissipated as geomagnetic activity. It is not clear *a priori* what functional relationship to expect between the power input and any of the many geomagnetic activity indices. However, it turns out from examination of available data the the am-index increases linearly with the power input given by (14). At our disposal we have 8741 three-hour averages of interplanetary magnetic field data during the interval 1965-1970. For each such three-hour interval we determine the angle α between the merging field lines using (15) and (26) through (31), and can then compute the corresponding value of $q(\alpha,s)$ using (13) and assuming a value for s. We now want to see how the am-index depends on $q(\alpha,s)$. Figure 10 shows that a linear relationship results for s=0.6. Other values of s do not result in a linear relationship as shown by dashed curves for s=0.5 and for s=0.7. These curves were constructed by assuming that the straight line for s=0.6 represents a functional relationship between am and α through the function $q(\alpha,s)$ and then applying that relation for the other values of s.

In constructing Figure 10 the data were divided into 16 classes of intervals of q such that all classes contain about the same number of data values. The average am-index and q-value for each class are then computed and plotted. This procedure tends to result in comparable statistical significance of each point plotted on the figure. Applying a similar procedure we also investigate how the am-index depends on the magnitude, B_I, of the interplanetary field. We find a linear relationship with the square of B_I as shown in Figure 11. Since such a dependence would follow if the am-index had a linear dependence on the power input given by (14), we are led to assume that a linear dependence on $q(\alpha,s)$ is the functional relation we are seeking. This implies that s should be chosen to be near 0.6.

Noting that the power input also depends on the solar wind speed, we should ascertain that the field magnitude and the solar wind speed are uncorrelated. An insert in Figure 11 shows the average field magnitude in 50km/sec bins of the solar wind speed. Only for the 2% of the data where the speed is less than 300km/sec do we find a field strength significantly different from the average value. It therefore seems reasonable to take Figures 10 and 11 as supporting the following relationship between the interplanetary magnetic field and geomagnetic activity measured by the am-index

$$am = am_1 + mB_I^2 q(\alpha,s) \tag{33}$$

where s=0.6, m=0.89 and $am_1 \approx 12$. Taking the most probable values for B_I and $q(\alpha,s)$ to be B_I = 4.5 nT and $q(\alpha,s) = 0.2647$ (i.e. $\alpha = 90^\circ$, s=0.6) we get

$$am = am_1 + 18.02\ q(\alpha,0.6) \tag{34}$$

$$am = am_1 + 0.236\ B_I^2 \tag{35}$$

both of which are very close to the best fit lines on Figures 10 and 11. The term am_1 could be interpreted as an indication of a component of activity that does not depend directly on the interplanetary magnetic field.

We now consider an ideal average interplanetary magnetic field and determine the expected diurnal and seasonal variations of geomagnetic activity that should result. We use our theory, which apparently does reasonably well in describing how the am-index depends in detail on the interplanetary magnetic field as we have just seen. In deriving eq.(20) we asserted that the average ecliptic latitude angle β of the interplanetary field is approximately zero. Because of the $7^{\circ}.25$ angle between the solar equator and the ecliptic, the ecliptic latitude angle of the average or ideal interplanetary field will have an annual variation between $-7^{\circ}.25$ and $+7^{\circ}.25$ approximately given by

$$\beta = 7^{\circ}.25 \sin (360^{\circ}(d-66)/365.24) \qquad (36)$$

The angle β will be zero near March 7 and near September 7. With reference to Figure 7 we should reinterpret the angle A as being the angle between the geomagnetic field in the merging region and the solar equatorial plane rather than the ecliptic plane. If we do this we may still set $\beta=0$ in the derivation of eq.(20) in order to arrive at the useful expressions (20) - (25). This is equivalent to rotating the field lines through the angle β, transforming the angle χ according to

$$\cos\chi' = \cos\chi\cos\beta + \cos\tau\sin\beta \qquad (37)$$

and computing A from $\cos A = \cos\chi'/\sin\psi$ (cf.eq.(26)).

We may now compute the function δ_{AT} for any given time of year and time of day by utilizing eq.(24). According to eq.(34) we can convert δ_{AT} into units of the am-index by multiplying by 18 and then compare the results with the variations shown in Figure 2 and 3. Table 1 gives the average δ_{AT} for each three-hour interval of the UT day for each month. Using this table, average diurnal variations of δ_{AT} x 18 were computed for each of the three seasons used in Figure 2 and are shown in Figure 12 as solid curves. Also shown in Figure 12 are the observed diurnal variation of the difference between the activity for away polarity and for toward polarity. The theoretical curves are in close agreement with the observed differences both in regard to phase and to amplitude, even including the systematic difference between the two solstices of the level of the difference values. A similar comparison of the annual variations as shown in the lower panel of Figure 12 also produces satisfactory agreement.

The influence of solar wind speed

The power input to the magnetcsphere has been discussed in terms of field line reconnection. The detailed agreement between the expected UT variations and observation indicates that reconnection is important in raising the magnetosphere to a more energetic state. It is less clear what happens when very unfavorable conditions for reconnection occur for extended periods. The non-zero term am_1 in the empirical relation (33) suggests that energy is always being transferred to the magnetosphere - even if reconnection has ceased or subsided to insignificance. The magnetotail is a permanent feature and the auroral oval never shrinks below a certain minimum size thus indicating that energy is being transferred to the magnetosphere by other processes in addition to reconnection, maybe the viscous or frictional interactions advocated several years ago (e.g., Axford, 1964). These interactions transfer momentum to the magnetosphere and influence the stand-off distance R_M for the subsolar point of the magnetopause, viz:

$$R_M = \left(F \frac{2B_E^2}{\mu_o \rho V^2} \right)^{1/6} R_E \qquad (44)$$

where B_E is the strength of the geomagnetic field at the subsolar point on the earth's surface. The factor F is experimentally determined to be 1.4 (Fairfield, 1971) and is determined through the details of the solar wind deflection by the geomagnetic field. Schield (1969) obtained $F=2.37/K$ where the parameter K is 1 for inelastic collision and 2 for total elastic reflection where the solar wind particles do not give up any kinetic energy. We now have $K=2.37/1.4=1.69$, indicating some energy transfer. About $(1.69-1)^2 = 0.5$ of the solar wind kinetic energy is transferred to the magnetosphere at the subsolar point. For an angle of incidence ν that is not zero a correspondingly smaller fraction, namely $\frac{1}{2}\cos^2\nu$, of the kinetic energy is transferred to the magnetosphere. The total amount of solar wind kinetic energy absorbed by the magnetosphere per second is then

$$K = \tfrac{1}{2} \cdot \frac{\pi}{4} R^2 \cdot (\tfrac{1}{2}\rho V^2) V = \frac{\pi}{16} R^2 \rho V^3 \qquad (45)$$

For quiet conditions with $R=25R_E$, $\rho=1.0 \times 10^{-20}$ kg/m^3, V=400 km/s, we get $K=3.2 \times 10^{12}$ watts=3.2 TW. By comparing this with the power input due to reconnection under quiet conditions, P=0.8 TW we would expect the term am_1 in eq.(34) to be about 4 times larger than the reconnection term $18\bar{q}$. The observed values $am_1 \approx 12$ and $18\bar{q} = 4.76$ are in reasonable agreement with this estimate, possibly indicating a slightly lower rate of kinetic energy transfer than derived above.

Using (44) and assuming that R scales as R_M we may interpret eq.(45) as implying that

$$K \sim \rho^{2/3} V^{7/3}$$

or

$$K \sim (\rho^2 V)^{1/3} V^2$$

The quantity $\rho^2 V$ is experimentally found to be rather constant on the average. This inverse statistical relationship between density and solar wind speed (e.g. Hundhausen et al., 1970) may be understood in terms of the occurrence of an extended rarefaction region following the leading edge of high-speed solar wind streams. In this low-density region the streaming speed generally attains its maximum value. Over the range of V from 300 km/s to 700 km/s the quantity $(\rho^2 V)^{1/3}$ changes only by a few percent. The net result is that we would expect the amount of kinetic energy transferred to the magnetosphere to vary as the square of the solar wind speed.

The power input owing to reconnection (eq.(13)) contains the factor $T^2 V$ thus depending on the length of T of the magnetotail and on the solar wind speed V. If we assume that $T^2 \sim V$, P will depend on V^2 just as K, and geomagnetic activity as such would then depend on the square of the solar wind speed. Such a dependence is indeed found empirically (cf. Figure 13). The data is consistent with the relation

$$am = am_3 V^2 \qquad (47)$$

where $am_3 = 9.2 \times 10^{-5}$ if V is expressed in km/s. Similar results were found by Murayama and Hakamada (1975) and noted in the very earliest studies of the relation between the solar wind speed and Kp (Snyder et al., 1963). At this point it should be emphasized that the relation (47) holds for the average activity levels. Because the release of magnetospheric energy has a sporadic character there may well be (and are, of course) intervals where the am-index is zero without requiring V = 0.

Agreement with the empirical relation (47) requires that the length of the magnetotail increases as $V^{\frac{1}{2}}$. This is reasonable as we would expect on general grounds that a higher solar wind speed should exert an increased drag on the tail resulting in a more extended tail. The reason for the specific relation $T \sim V^{\frac{1}{2}}$ is not clear at the present.

The detailed quantitative description of at least one component of geomagnetic activity using the reconnection model is encouraging in spite of the fact that it forces us to accept that at least one other component exists. The component we have discussed in detail already - depending critically on the magnitude and direction of the interplanetary magnetic field - does not have significant seasonal or diurnal variations when a large number of days are considered without regard to the sector polarity. What is observed in this case is the well-known variations that depend on the angle ψ between the solar wind flow direction and the earth's dipole axis. As pointed out by Boller and Stolov (1970) these variations depend on $\cos^2\psi$. Using solar - wind plasma data for the interval 1965-1970 (a total of 6410 three-hour intervals) we divided the data into two groups such that the first group had a solar wind speed less than average and the second group had a higher than average speed. For each group the average am-index was computed for each three-hour interval of the UT-day for each month. The mean speed for each group is 371 km/s and 511 km/s respectively. According to eq. (47), the quantity $\bar{V}^2/am$ should be independent of $\bar{V}$. Figure 14 shows a plot of $\bar{V}^2/am$ as function of $\cos^2\psi$ for each group. The best-fit straight line corresponds to the relation

$$am = 1.09 \times 10^{-4} V^2/(1+1.7\cos^2\psi) \qquad (48)$$

and confirms the inverse relation with $\cos^2\psi$.

The mechanism responsible for the $\cos^2\psi$ dependence is not clear. The Kelvin-Helmholtz instability of the boundary between two magneto-hydrodynamic fluids in relative motion has been suggested as a possible cause of instability of the magnetopause leading to release of some of the energy stored in the magnetotail (e.g. Boller and Stolov, 1970). An approximate instability criterion developed by Chandrasekhar (1961) has been applied to the magnetopause by Boller and Stolov in the form

$$U^2 > \frac{\rho_M+\rho_G}{2\mu_o\rho_M\rho_G}\,(B_M^2\cos^2\psi_M+B_G^2\cos^2\psi_G) \qquad (49)$$

where subscript M denotes magnetosheath values and G stands for magneto-spheric values (just inside the magnetopause). U is the streaming velocity of the solar wind at the magnetopause and ψ is the angle between the local streaming velocity vector and the magnetic induction field B. The symbol ρ refers to the mass density. Following Boller and Stolov we note that the flanks of the magnetosphere (dawn and dusk regions) are the most likely places for instability to occur because ψ_G is close to 90^o, thereby minimizing the righthand side of ineq.(49). At the flanks the geometry is such that $\psi = -\psi_G$ is the angle between the solar wind direction and the dipole axis. Let us now assume that $\rho_M \simeq \rho_G \simeq \rho$ and introduce $s = B_M/B_G$ and the Alfvén speed $V_A = B_M/\sqrt{\mu_o\rho}$. Hence we can rewrite the instability criterion as

$$M_A^2 = U^2/V_A^2 > (1+\left(\frac{1}{s}\right)^2\cos^2\psi) \qquad (50)$$

If the Alfvénic Mach-number M_A exceeds some value depending on $\cos^2\psi$ the magnetopause may be unstable against the growth of the Kelvin-Helmholtz instability maybe resulting in a greater stress on the magnetosphere. No further mechanism is available and it remains possible that other basic processes than the instability may be operative in producing the observed $\cos^2\psi$ modulation. If we identify the coefficient of $\cos^2\psi$ in eq. (48) with the quantity $\left(\frac{1}{s}\right)^2$ we find $s = 0.76$. Although $s \simeq 0.6$ at the sunward side of the magnetosphere it is not unreasonable to find a somewhat larger value at the flanks as s should approach unity as we go downstreams along the

tail. Whatever the mechanism for generating the $\cos^2\psi$ dependence is, there is no doubt that such an additional process must be invoked to account for the observed variations. The reconnection model, while accounting nicely for some part of geomagnetic activity, fail to explain the classical semi-annual and diurnal variations of the activity.

Rudneva and Feldshsteyn (1973) have shown that the stand-off distance R_M depends on the geomagnetic activity index Kp. When Kp was large, R_M was small. Conceivably the causal relation is reversed. Because the R_M-values used by Rudneva and Feldshsteyn were corrected for changes in solar wind pressure, they interpreted their results in terms of erosion of the day-side magnetosphere due to reconnection with southward interplanetary field, subsequently associated with increases in geomagnetic activity. According to the data presented by Rudneva and Feldshsteyn, the am-index would depend linearly upon $1/R_M^2$. It is interesting to note that the size of the magnetosphere (as given by R_M) depends on the dipole tilt and thus has seasonal and diurnal variations of the order of 10%. One could speculate that some unknown process modulates geomagnetic activity depending on the size of the magnetosphere. Maybe the internal stability decreases if the magnetosphere is compressed. In any case, the strength B_E of the geomagnetic field at the subsolar point on the earth's surface is given by

$$B_E = B_o(1 + 3\cos^2\psi)$$

which combined with eq.(44) yields

$$R_M^2 \sim (1 + 3\cos^2\psi)^{2/3}$$

The righthand side is within 1 percent identical to the denominator of eq. (48) over the range of possible values of ψ. The observations are thus also consistent with the assumption that geomagnetic activity depends inversely on the square of the size of the magnetosphere. No processes are yet identified as being responsible for such a relationship but may be found if sought after.

Functional description of geomagnetic activity

The separation of the two mechanisms responsible for geomagnetic activity in connection with the theoretical considerations laid out in the previous sections suggest the following functional description of the am-index

$$am = \frac{a + bB_I^2 q(\alpha,s)}{1+c\ \cos^2\psi}\ V^2 \qquad (51)$$

where a,b, and c are constants or nearly so. The various empirical relations eqs. (34), (35), (47), and (48) suggest the following values for the coefficients:

$$a = 0.523 \times 10^{-4}$$
$$b = 0.0556 \times 10^{-4}$$
$$c = 1.71$$

if V is expressed in km/s and B_I in nT. These coefficients are obtained from spacecraft data covering the interval 1965-1970 assuming a uniform coverage. More detailed and extensive data analysis will probably result in improved values for a,b, and c. Using yearly average values of $q = 0.2647$ and $\cos^2\psi = 0.0943$, eq. (51) becomes

$$am = (0.45 + 0.0127\ B_I^2)\ V^2 \times 10^{-4} \qquad (52)$$

It is of interest to verify that the coefficients a,b, and c are the same for a wide range of V and B_I. The available data with simultaneous measurements of V and B_I was divided into three ranges of V and three ranges of B_I forming a total of 3 x 3 = 9 groups in such a way that each group contains approximately the same number of three-hour averages (about 500). The average observed am-index was then computed for each group. The result is shown in Table 2a. Using eq. (52) and the average values of V and B_I for each group the calculated values of am are shown in Table 2b. The rms error is only about 4% and the agreement is uniform over the table verifying the constancy of the coefficients of (52). A graphical representation of this result is shown in Figure 15. The quantity am/V^2 should depend linearly on B_I^2 with the same slope and intercept for each range of V. The straight line, depicting the relationship (52), is seen to be an excellent fit to the data

points for each group, again verifying the constancy of the coefficients of eq. (51).

The importance of a precise functional relationship between solar wind parameters and geomagnetic activity such as eq. (51), lies in the possibility of utilizing the more than century-long monitoring of geomagnetic disturbances to investigate solar-cycle variations and even secular variations of the properties of the solar wind. This problem has recently been discussed by Russell (1975) but has long been a driving force behind the tedious work of recording and deriving magnetic activity indices.

Conclusion

We have shown that two different mechanisms transfer energy to the magnetosphere. One mechanism depends critically on the direction and magnitude of the interplanetary magnetic field and can be quantitatively explained in terms of reconnection at the dayside magnetopause. The other mechanism may be related to viscous or frictional interactions exerting tangential stresses on the magnetotail but does not depend on the interplanetary magnetic field maybe except in a passive role of being a necessary element in giving the solar wind fluid properties. Both mechanisms depend strongly on the solar wind speed. Under normal conditions both mechanisms supply comparable amounts of energy to the magnetosphere. A strong southward directed interplanetary magnetic field results in a large increase of the energy gained by reconnection making this mechanism dominant. Large Universal Time and seasonal variations are found in the efficiency of the reconnection process depending on the sign of the azimuthal component of the interplanetary magnetic field. For intervals of time having the same number of days of both sector polarities, these UT and seasonal variations practically even out to an almost uniform level of activity. The energy transferred to the magnetosphere by the two mechanisms is modulated by the tilt of the geomagnetic dipole axis to the direction of the solar wind velocity vector, being at a maximum for a 90° tilt. The Kelvin-Helmholtz instability at the flanks of the magnetopause could be responsible for an increased drag on the tail.

A functional description of geomagnetic activity is given that is understandable in terms of physical mechanisms. The relationship (51) expresses explicitly the influence of the two energy input mechanisms and of the $\cos^2\psi$-modulation.

We realize that the unified description of geomagnetic activity presented here may not be unique and indeed that much more study is needed to clarify finer points of the theory. Nevertheless, we feel that the observational evidence presented are strong enough that the present paper may become a starting point for further investigations of the causes of geomagnetic activity. As is often the case, the separation of a complex phenomenon into several distinctly different but simpler

components could lead to rapid progress in our understanding of the problem.

Acknowledgements.

The development of the present paper has profited much from detailed discussions and constant encouragement from John M. Wilcox. I thank P.N. Mayaud, T. Murayama and A.J. Dessler for comments on the manuscript. J.H. King at the National Space Science Data Center and W. Paulishak at World Data Center A were most helpful in obtaining the interplanetary and geomagnetic data. I would like to express appreciation of the work carried out at geomagnetic observatories, past and present, all over the world. The continuous recording and careful reduction of geomagnetic variations, sometimes performed under extremely adverse conditions, was started well over a century ago and is today becoming an increasingly important tool of research into the environment of spaceship Earth. The present research was supported in part by the Office of Naval Research under Contract N00014-76-C-0207, by the National Aeronautics and Space Administration under Grant NGR 05-020-559, and by the Atmospheric Sciences Section of the National Science Foundation under Grant ATM74-19007.

References.

Axford, W.I., 1964: Viscous interaction between the solar wind and the earth's magnetosphere. Planet. Space Sci., 12, 45.

Bartels, J., N.H. Heck, and H.F. Johnston, 1939: The three-hour-range index measuring geomagnetic activity. Terr. Mag. Atm. Elect., 44, 411.

Broun, J.A., 1874: Observations of magnetic declination at Trevandrum and Agustia Malley 1852-1869. Trevandrum Magnetical Observations, 1, 95.

Boller, B.R. and H.L. Stolov, 1970: Kelvin-Helmholtz instability and the semiannual variation of geomagnetic activity. J. Geophys. Re., 75, 6073.

Boller, B.R. and H.L. Stolov, 1973: Explorer 18 study of the stability of the magnetopause using a Kelvin-Helmholtz instability criterion. J. Geophys. Res., 78, 8078.

Burch, J.L., 1973: Effects of interplanetary magnetic sector structure on auroral zone and polar cap magnetic activity. J. Geophys. Res., 78, 1047.

Burch, J.L., 1974: Observations of interactions between interplanetary and geomagnetic fields. Rev. Geophys. Space Phys., 12, 363.

Chandrasekhar, S., 1961: Hydrodynamic and Hydromagnetic Stability, Oxford University Press, New York.

Fairfield, D.H., 1967: The ordered magnetic field of the magnetosheath. J. Geophys. Res., 72, 5865.

Fairfield, D.H., 1971: Average and unusual locations of the earth's magnetopause and bow shock. J. Geophys. Res., 76, 6700.

Gonzales, W.D. and F.S. Mozer, 1974: A quantitative model for the potential resulting from reconnection with an arbitrary interplanetary magnetic field. J. Geophys. Res., 79, 4186.

Hundhausen, A.J., S.J. Bame, J.R. Asbridge, and S.J. Sydoriak, 1970: Solar wind proton properties: Vela 3 observations from July 1965 to June 1967. J. Geophys. Res., 75, 4643.

Mayaud, P.N., 1967: Calcul préliminaire d'indices Km, Kn et Ks ou am, an et as, mesures de l'activité magnétique à l'échelle mondiale et dans les hémisphères Nord et Sud. Ann. Géophys., 23, 585.

Mayaud, P.N., 1970: Sur quelques propriétés de l'activité magnétique déduites de l'analyse d'une série de neuf années des indices Kn, Ks et Km; II. Les diverse composantes "temps universel" dans chaque hémisphère, de la variation journalière de l'activité. Ann. Géophys., 26, 313.

McIntosh, D.H., 1959: On the annual variation of magnetic disturbance. Phil. Trans. Roy. Soc. Lond., Series A, 251, 525.

Meyer, J., 1974: Harmonic analysis of geomagnetic indices Km. Ann. Geophys., 30, 503.

Murayama, T. and K. Hakamada, 1975: Effects of solar wind parameters on the development of magnetospheric substorms. Planet. Space Sci., 23, 75.

Rudneva, N.M. and Ya. I. Feldshsteyn, 1973: Position of the boundary of the magnetosphere during 1963-68. Geomagn. i Aeronomiya, 13, 96.

Russell, C.T. and R.L. McPherron, 1973: Semiannual variation of geomagnetic activity. J. Geophys. Res., 78, 92.

Russell, C.T. and R.L. McPherron, 1974: Reply to comment on 'Semiannual variation of geomagnetic activity'. J. Geophys. Res., 79, 1132.

Russell, C.T., 1975: On the possibility of deducing interplanetary and solar parameters from geomagnetic records. Solar Phys., 42, 259.

Saito, T., 1972: Recurrent magnetic storms in relation to the structure of solar and interplanetary magnetic fields. Rep. Ionos. Space Res. Japan, 26, 245.

Schatten, K.H. and J.M. Wilcox, 1967: Response of the geomagnetic activity index Kp to the interplanetary magnetic field. J. Geophys. Res., 72, 5185.

Shield, M.A., 1969: Pressure balance between solar wind and magnetosphere. J. Geophys. Res., 74, 1275.

Siebert, M., 1971: Maßzahlen der erdmagnetischen Aktivität, in Handbuch der Physik, vol. XLIX/3, (S. Flügge, ed.), Springer, Berlin, 206.

Snyder, C.W., M. Neugebauer, and U.R. Rao, 1963: The solar wind velocity and its correlation with cosmic-ray variations and with solar and geomagnetic activity. J. Geophys. Res., 68, 6361.

Sonnerup, B.U.Ö., 1974: Magnetopause reconnection rate. J. Geophys. Res. 79, 1546.

Svalgaard, L., 1972: Interplanetary magnetic structure 1926-1971. J. Geophys. Res., 77, 4027.

Vasyliunas, V.M., 1975: Theoretical models of magnetic field line merging, I. Rev. Geophys. Space Phys., 13, 303.

Walters, G.K., 1964: Effect of oblique interplanetary magnetic field on shape and behavior of the magnetosphere. J. Geophys. Res., 69, 1769.

Wilcox, J.M., 1968: The interplanetary magnetic field: Solar origin and terrestrial effects. Space Sci. Rev., 8, 258.

Wilcox, J.M., 1972: Inferring the interplanetary magnetic field by observing the polar geomagnetic field. Rev. Geophys. Space Phys., 10, 1003.

Wilcox, J.M. and D.S. Colburn, 1972: Interplanetary sector structure at solar maximum. J. Geophys. Res., 77, 751.

TABLE 1

	1	2	3	4	5	6	7	8	Day
JAN	-0.310	-0.125	0.081	0.162	0.087	-0.091	-0.273	-0.365	-0.104
FEB	-0.533	-0.382	-0.200	-0.118	-0.185	-0.348	-0.505	-0.576	-0.365
MAR	-0.642	-0.521	-0.367	-0.293	-0.354	-0.503	-0.631	-0.678	-0.499
APR	-0.657	-0.539	-0.393	-0.321	-0.382	-0.534	-0.658	-0.695	-0.522
MAY	-0.581	-0.439	-0.276	-0.194	-0.258	-0.436	-0.588	-0.632	-0.424
JUN	-0.386	-0.216	-0.032	0.063	0.004	-0.194	-0.388	-0.451	-0.200
JUL	-0.087	0.090	0.273	0.365	0.133	0.133	-0.073	-0.154	0.108
AUG	0.185	0.349	0.505	0.576	0.537	0.387	0.205	0.124	0.358
SEP	0.351	0.500	0.630	0.677	0.641	0.519	0.365	0.291	0.497
OCT	0.383	0.535	0.659	0.696	0.656	0.538	0.391	0.318	0.522
NOV	0.266	0.442	0.594	0.637	0.581	0.440	0.276	0.194	0.429
DEC	-0.003	0.195	0.389	0.452	0.379	0.208	0.024	-0.072	0.196
YEAR	-0.168	-0.009	0.155	0.225	0.169	0.010	-0.155	-0.225	

0 3 6 9 12 15 18 21 24^hUT

Seasonal and diurnal variation of the function δ_{AT} related to the difference in power input to the magnetosphere on away days and on toward days.

TABLE 2a

	B_I<4.0 nT	4.0≤ B_I<6.2	B_I≥6.2	
V<385 km/s	6.5	9.6	15.4	$\bar{V}$ = 346
385≤V<465	10.4	14.2	25.3	$\bar{V}$ = 424
V≥465	17.1	22.2	42.2	$\bar{V}$ = 536
	$\bar{B}_I$ = 3.15	$\bar{B}_I$ = 5.04	$\bar{B}_I$ = 8.59	

Average observed am-index for 9 different groupings of interplanetary parameters V (solar wind speed) and B_I (magnetic field strength).

TABLE 2b

6.9	9.2	16.6
10.4	13.9	24.9
16.5	22.2	39.9

Computed values of am-index for the same groups as in Table 2a using eq.(52).

Figure Captions.

Figure 1 Universal time variations of geomagnetic indices an, am, and as. Interplanetary magnetic field polarity (measured by spacecraft during 1962-1970) was used to divide the data into two groups Away polarity (open circles) and Toward polarity (solid dots). In the righthand panel the difference between the universal time variations (away-toward) is shown.

Figure 2 Universal time variations of the difference between the am-index on away-days (A) and on toward-days (T) are shown in the lefthand panel, while the average variations $[(A+T)/2]$ are shown in the righthand panel. The variations are shown for different seasons as indicated on the figure.

Figure 3 Seasonal variation of the difference in activity between away and toward polarity (A-T) and of the average activity level $[(A+T)/2]$. The difference shows an annual variation while the average shows a semiannual variation.

Figure 4 Universal time variations of am for different polarities and seasons.

Figure 5 Topology of magnetic field lines near the earth. The thick lines mark the separatrix. Various regions as discussed in the text are indicated. The dipole axis is in the plane of the paper and the sun is to the left.

Figure 6 Geomagnetic field vector $\underline{B}_G$ and interplanetary magnetic field $\underline{B}_I$ at the reconnection line (X line). The antiparallel component $\underline{B}$ of the interplanetary field is indicated.

Figure 7 Equatorial plane view of the draping of the interplanetary magnetic field around the nose of the magnetosphere. The situation is shown here for away polarity.

Figure 8 Field line geometry at the nose of the magnetosphere as seen from the sun for different orientations of the interplanetary magnetic field (dashed arrow) and the geomagnetic field (solid arrow marked NS). The ecliptic is indicated by EE. Definition of the angles A, β and α are shown.

Figure 9 Geometrical relations between rotation axis, dipole axis and orbital parameters:

OG = rotation axis of the earth,
OM = geomagnetic dipole axis,
S = stagnation point at nose of magnetosphere
O = center of earth,
$i = \widehat{MG}$, $\epsilon = \widehat{PG}$, $\lambda = \widehat{TU}$, $\widehat{ST} = 90^{\circ}$,
$\psi = \widehat{SM}$, $\chi = \widehat{TM}$, $\zeta = \widehat{MU}$, $\widehat{PU} = 90^{\circ}$,
$h = \angle PGM$, $A = \angle TSM$, $u = \angle SUM$, $\angle UGM = 180^{\circ} - h$,
$\angle MUG = 90^{\circ} - u$, $\widehat{SU} = 90^{\circ} - \lambda$, $\angle MUT = 180^{\circ} - u$,
$\widehat{GU} = 90^{\circ} - \epsilon$, $\tau = \widehat{PM}$.

Figure 10 Relation between the am-index and the q-parameter (defined as shown) for s = 0.6. The data points fit the solid s=0.6 line. For other values of s, the data points should fall along the curved, dashed lines. The data has been divided into 16 bins with about the same number of measurements in each. The angle α is derived from the measured solar-ecliptic latitude β as shown on Figure 8.

Figure 11 Relation between the am-index and the corresponding three-hour average of the magnitude B_I of the interplanetary magnetic field. The straight line represents the linear fit shown on the figure. An insert shows that for most of the data the solar wind speed V and B_I are almost uncorrelated. The exception is the very lowest field strengths that seem to be observed together with low solar wind speed values. The data points corresponding to these low fields are shown as open circles. Again the data has been divided into bins of about equal number of measurements.

Figure 12 Comparison of computed (solid curves) and observed (dots) universal time (upper panel) and seasonal (lower panel) variations of the geomagnetic activity index am. The differences between the variations during away polarity and during toward polarity are shown.

Figure 13 Relation between solar wind speed V and the am-index. Due to the quadratic form of the relation the square-root of am is plotted. The dashed line (forced to go through the origin) is given by the relation shown in the figure.

Figure 14 Dependence of the am-index on the tilt of the dipole axis ψ. The quantities plotted are $\bar{V}^2/am$ and $\cos^2\psi$ for the two groups of data with different solar wind speed $\bar{V}$. See text for details. The straight line is given by the relation shown and is the least squares best fit to the combined set of data points.

Figure 15 Graphical verification of the functional relation between geomagnetic activity am and interplanetary field strength B_I for three groups of solar wind speed V (see text).

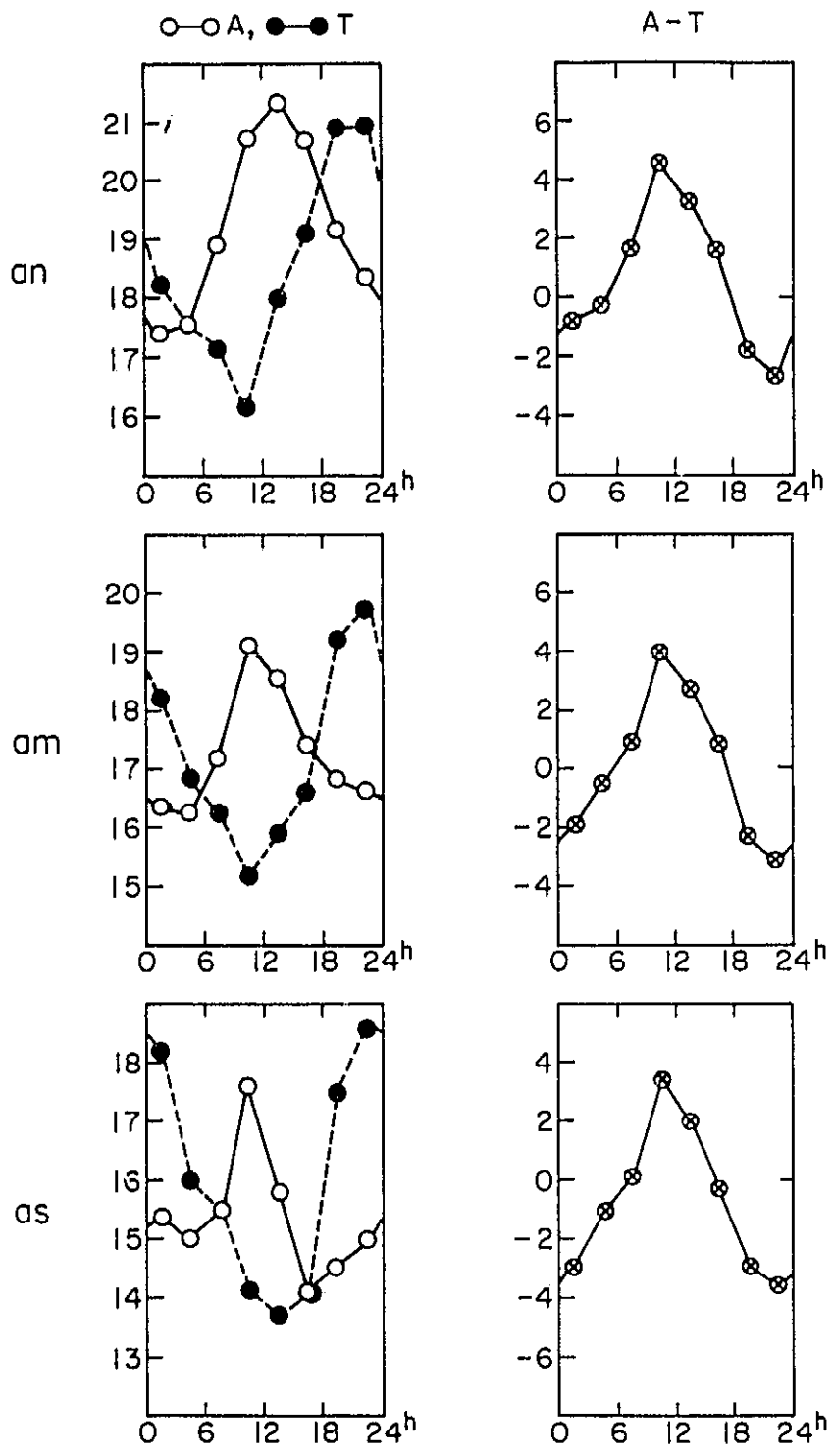

Figure 1

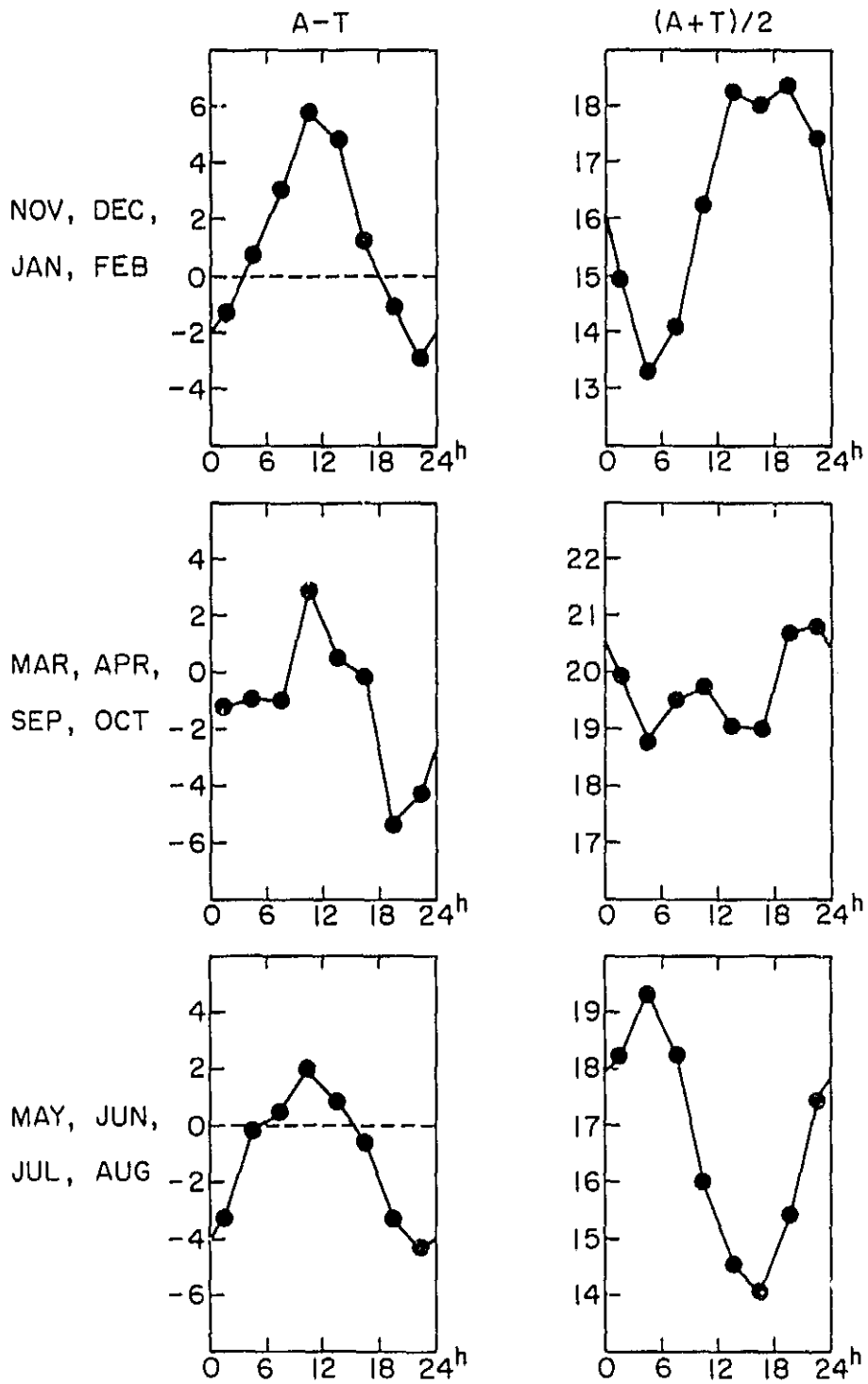
A-T
(A+T)/2
NOV, DEC,
JAN, FEB
MAR, APR,
SEP, OCT
MAY, JUN,
JUL, AUG
0 6 12 18 24h

Figure 2

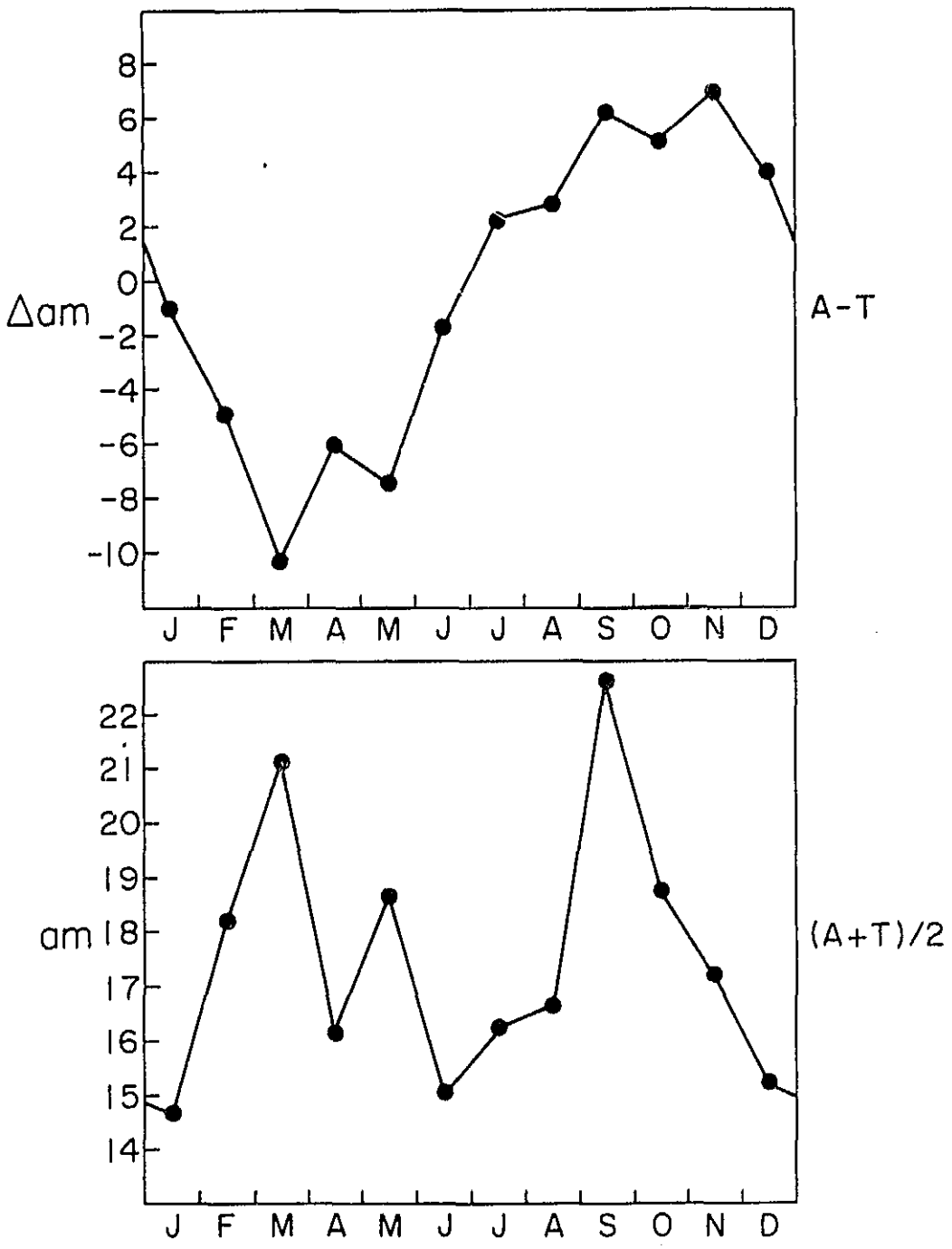
8
6
4
2
0
-2
-4
-6
-8
-10
Δam
A-T
J F M A M J J A S O N D
22
21
20
19
18
17
16
15
14
am
(A+T)/2
J F M A M J J A S O N D

Figure 3

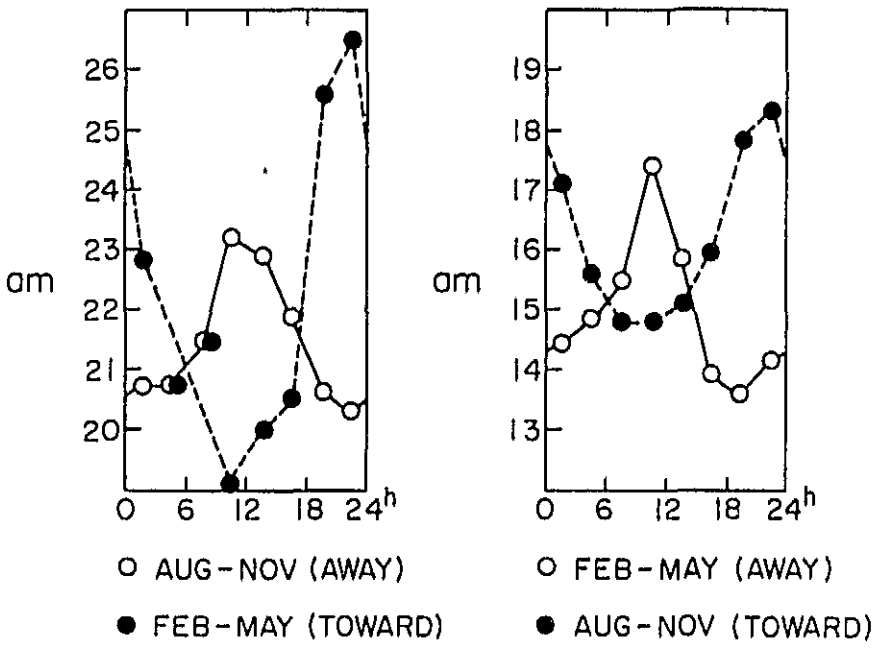

Figure 4

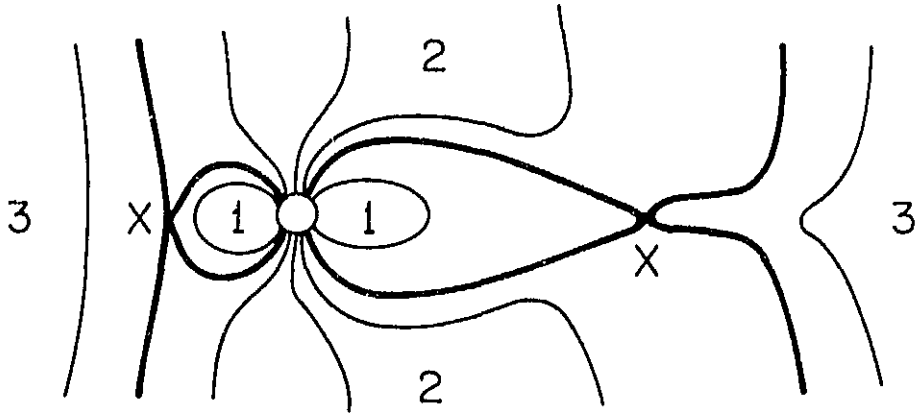

Figure 5

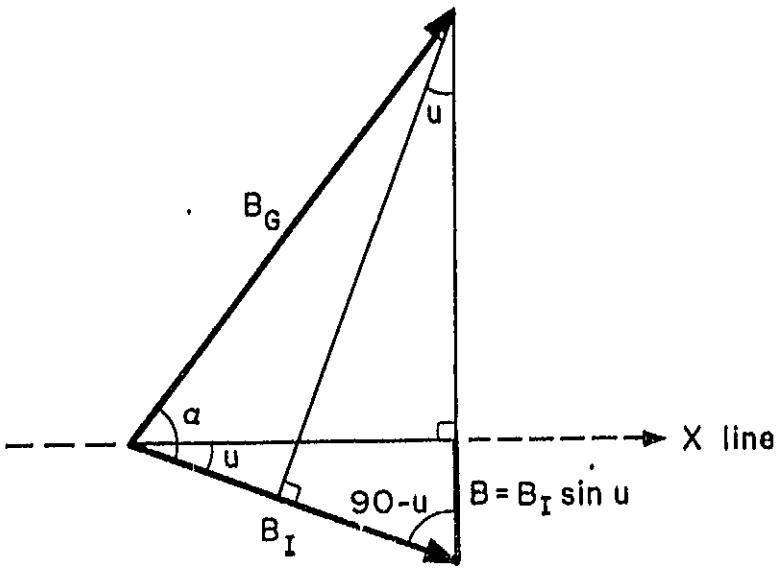

Figure 6

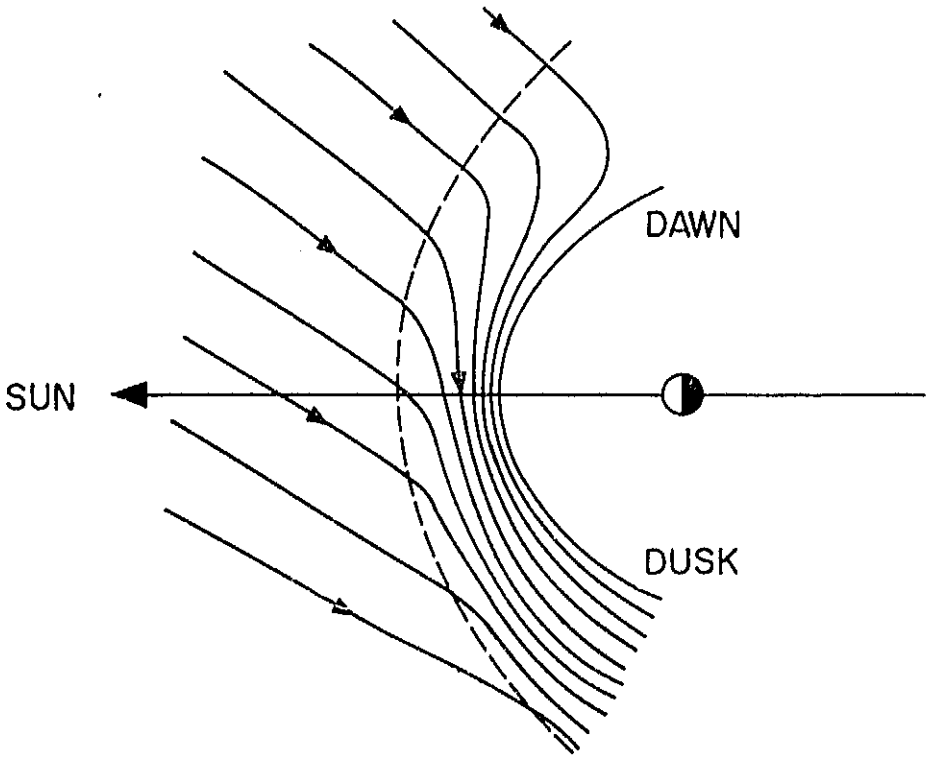

DRAPING OF IMF AROUND NOSE OF MAGNETOSPHERE

Figure 7

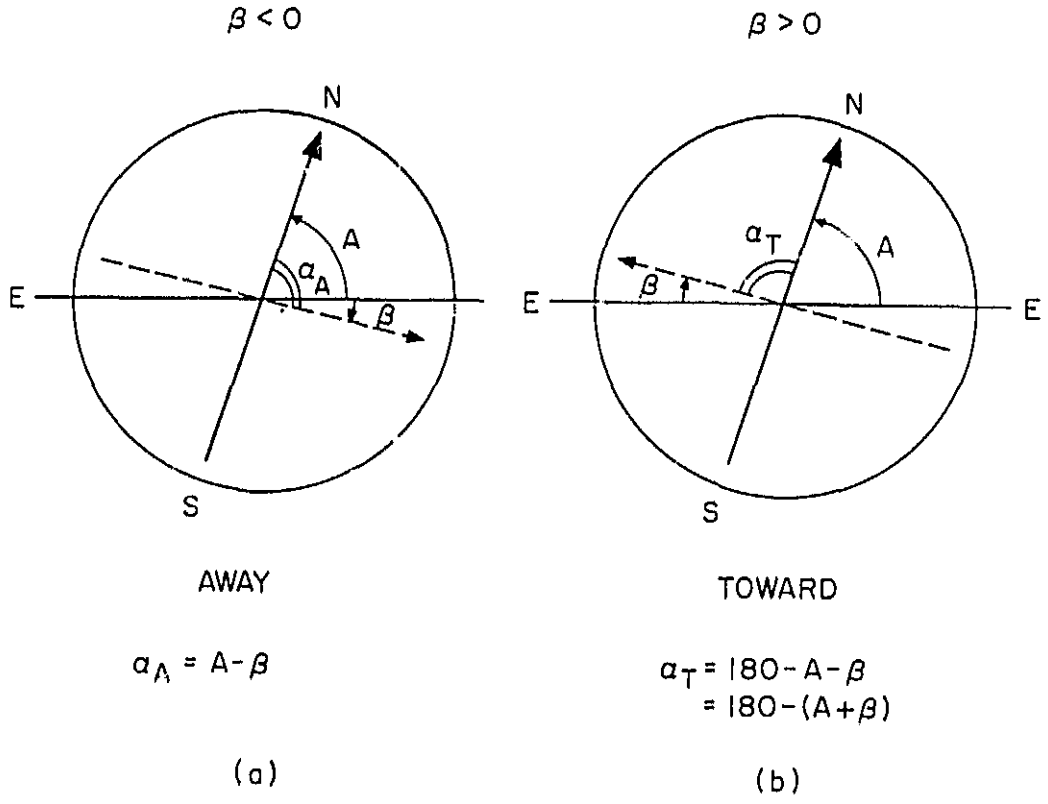

Figure 8

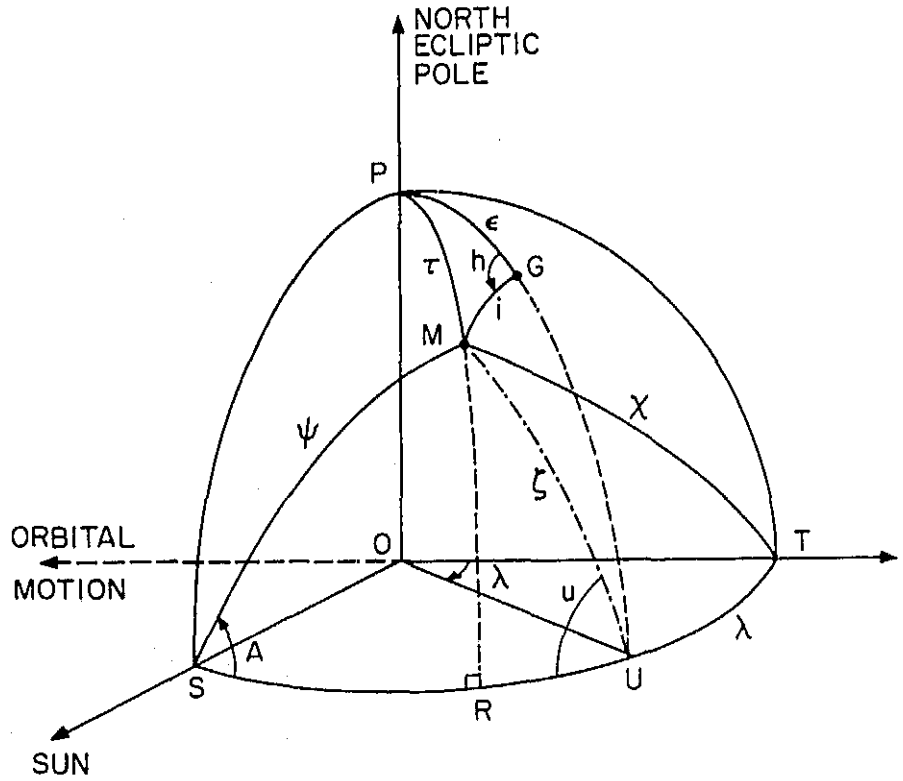

Figure 9

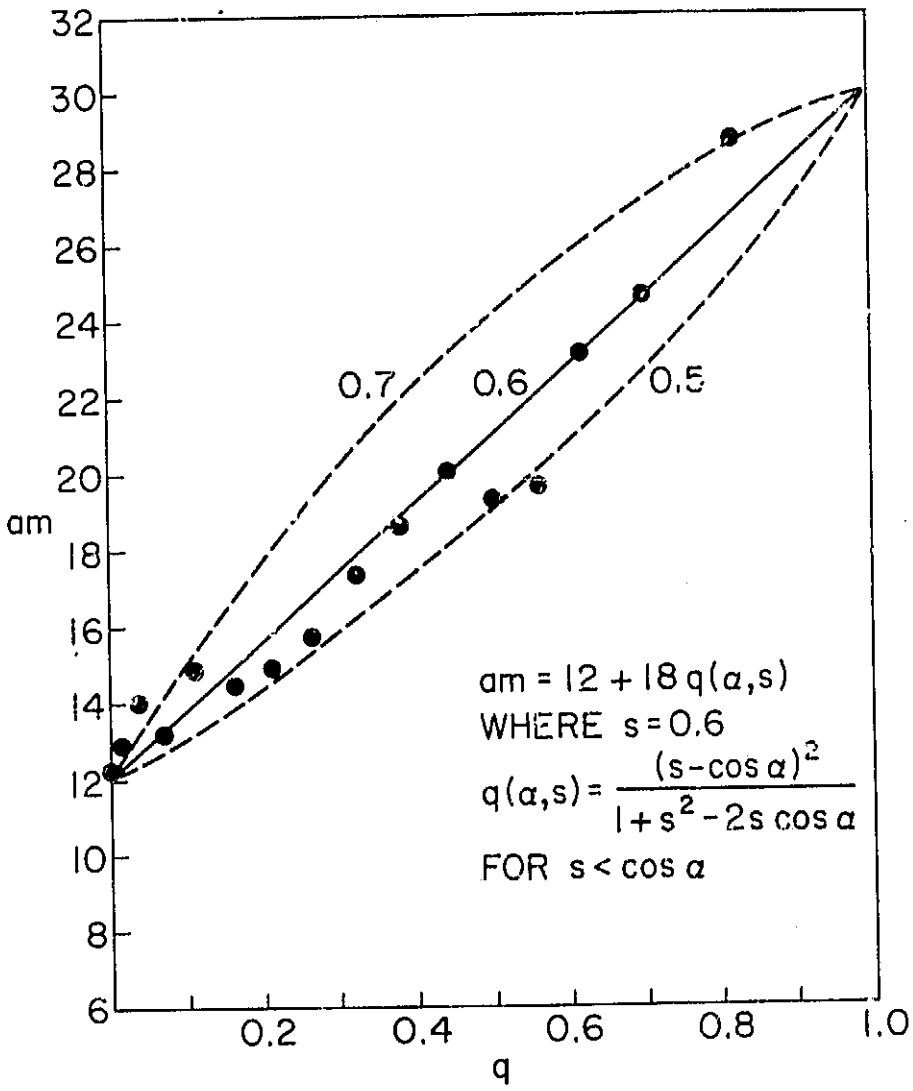
32
30
28
26
24
22
20
18
16
14
12
10
8
6
am
0.2
0.4
0.6
0.8
1.0
q
0.7
0.6
0.5
am = 12 + 18 q(α,s)
WHERE s = 0.6
q(α,s) = (s-cos α)² / (1+s²-2s cos α)
FOR s < cos α

Figure 10

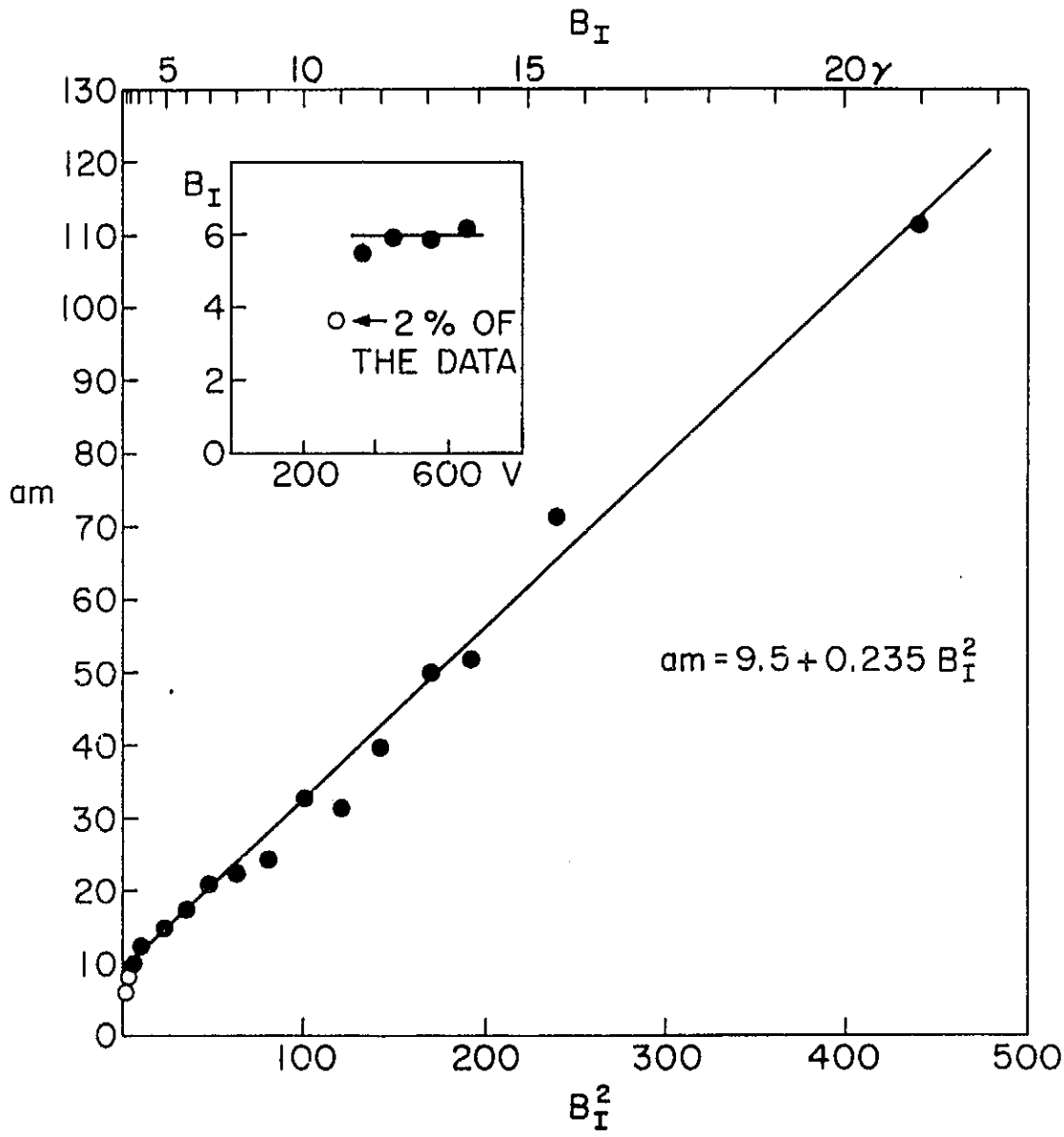
B_I
5
10
15
20γ
130
120
110
100
90
80
70
60
50
40
30
20
10
0
am
B_I
6
4
2
0
200
600 V
o ← 2 % OF
THE DATA
am = 9.5 + 0.235 B_I^2
100
200
300
400
500
B_I^2

Figure 11

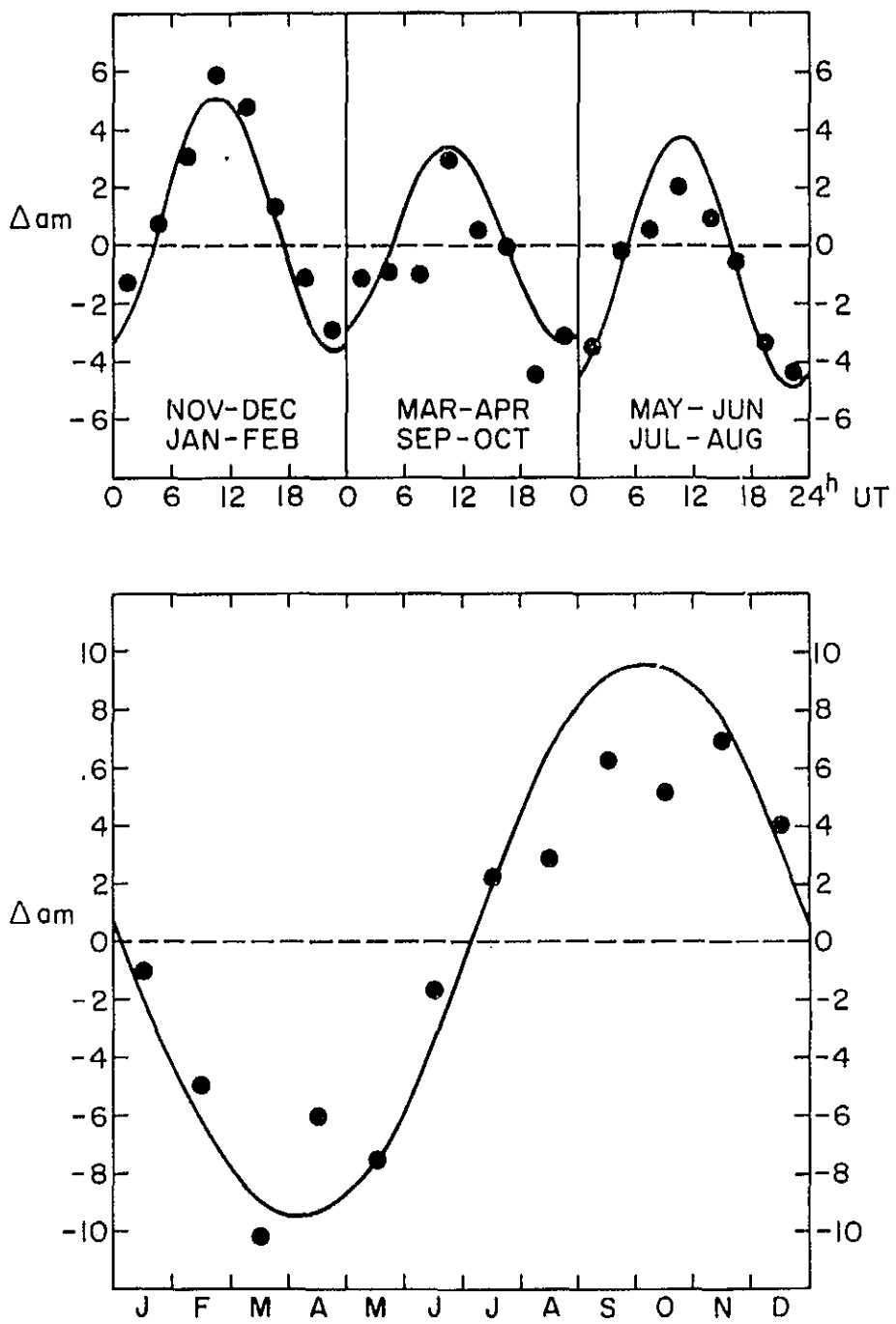
Δam
NOV-DEC
JAN-FEB
MAR-APR
SEP-OCT
MAY-JUN
JUL-AUG
0 6 12 18 0 6 12 18 0 6 12 18 24h UT
J F M A M J J A S O N D

Figure 12

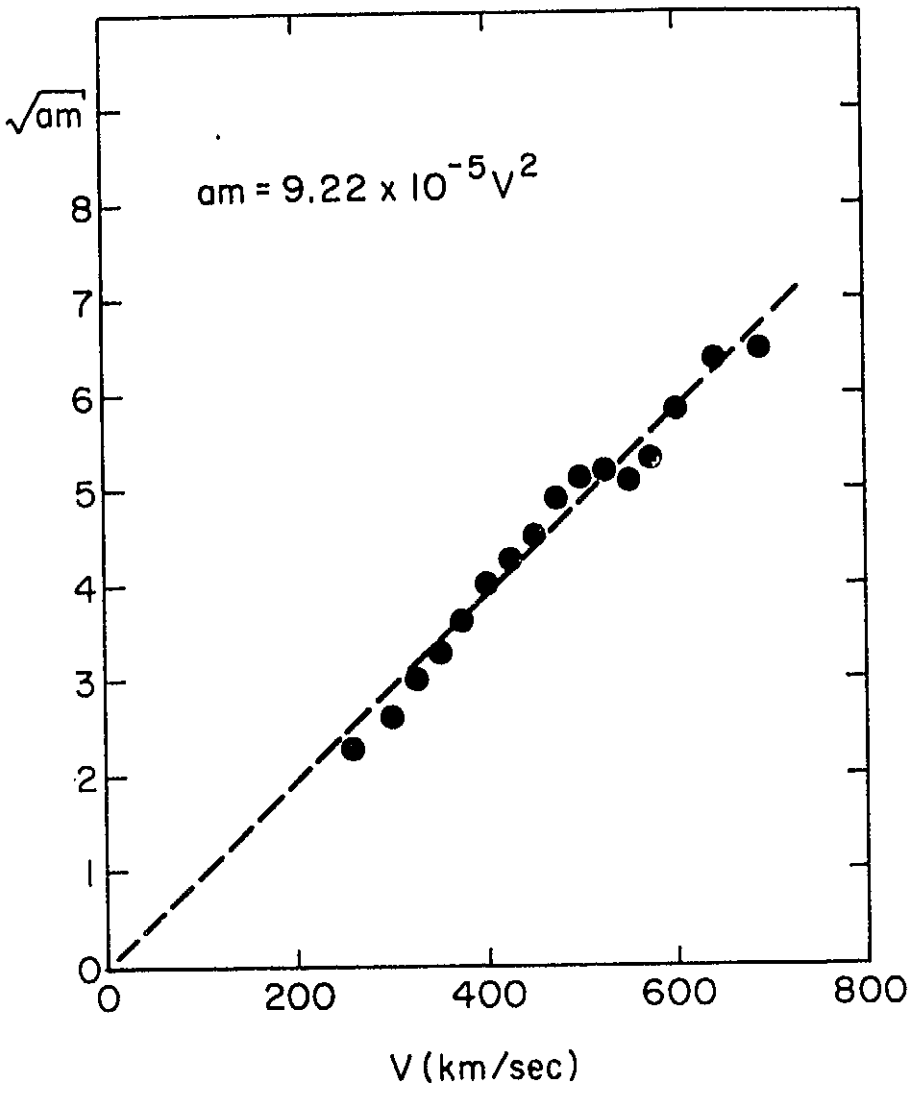

Figure 13

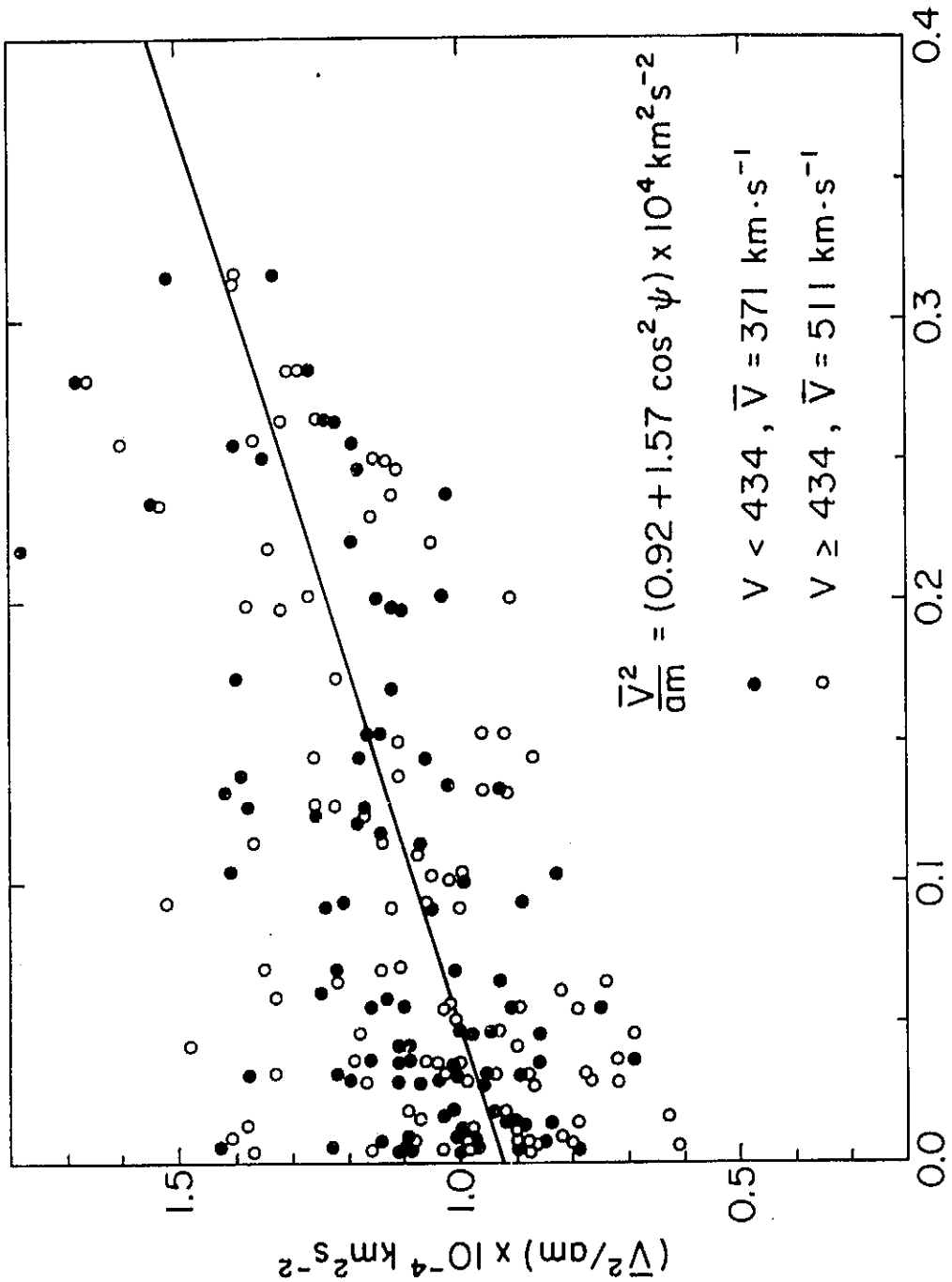
$\frac{\overline{V}^2}{am} = (0.92 + 1.57\cos^2\psi) \times 10^4 km^2 s^{-2}$
$V < 434$, $\overline{V} = 371$ km·s^{-1}
$V \geq 434$, $\overline{V} = 511$ km·s^{-1}
$(\overline{V}^2/am) \times 10^{-4}$ km^{2}s^{-2}
$\cos^2\psi$
0.0
0.1
0.2
0.3
0.4
0.5
1.0
1.5

Figure 14

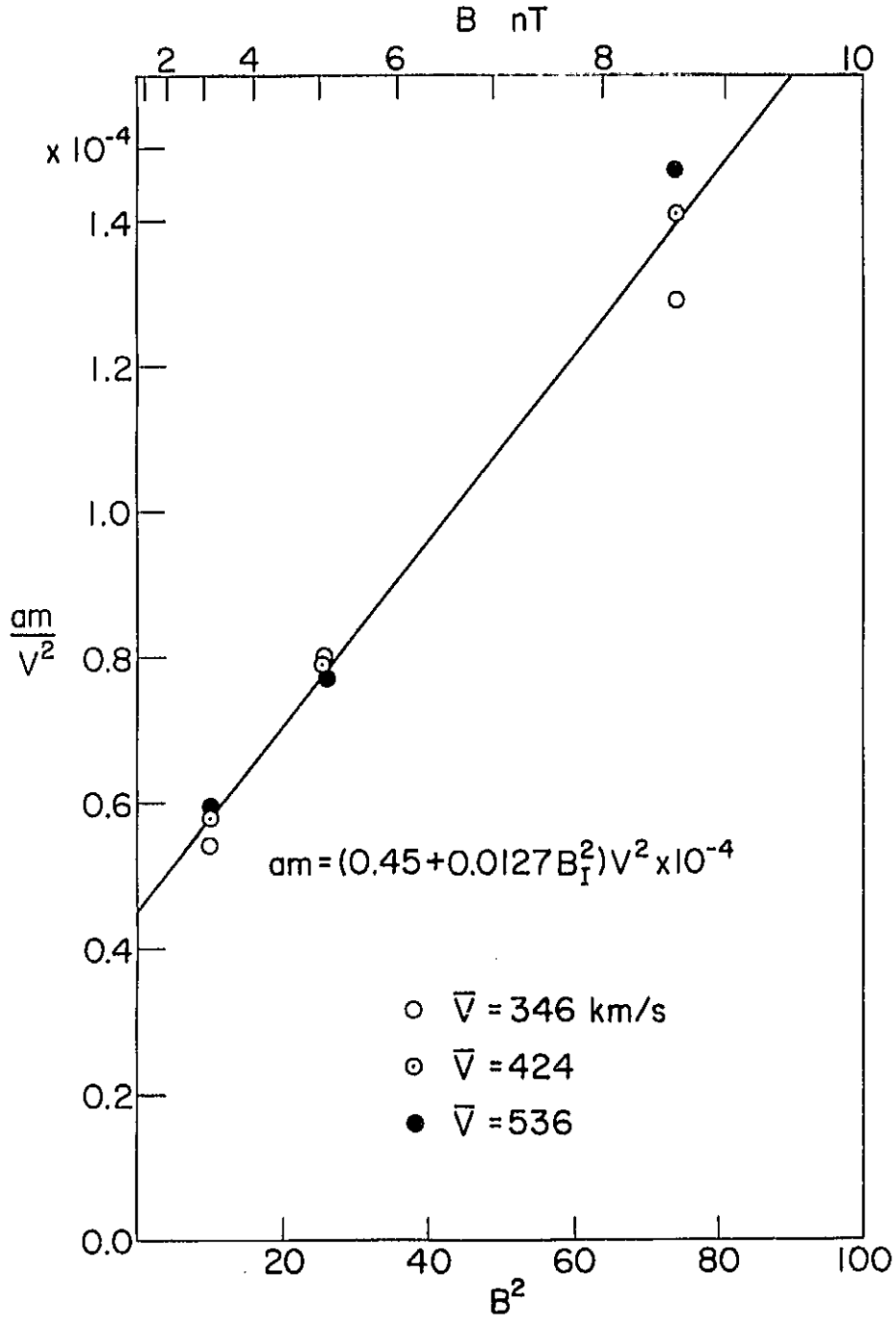
B nT
2
4
6
8
10
x 10⁻⁴
1.4
1.2
1.0
am/V²
0.8
0.6
0.4
0.2
0.0
am = (0.45 + 0.0127 B_I²) V² x 10⁻⁴
V̄ = 346 km/s
V̄ = 424
V̄ = 536
20
40
60
80
100
B²

Figure 15